2020

OPTIMUM DESIGN OF SHIMMED FOIL BEARING CONSIDERING ROTORDYNAMIC STABILITY

Venkata Sai Jyothish Atluri

OPTIMUM DESIGN OF SHIMMED FOIL BEARING CONSIDERING ROTORDYNAMIC STABILITY

by

VENKATA SAI JYOTHISH ATLURI

Presented to the Faculty of the Graduate School of

The University of Texas at Arlington in Partial Fulfillment

of the Requirements

for the Degree of

MASTER OF SCIENCE IN MECHANICAL ENGINEERING

THE UNIVERSITY OF TEXAS AT ARLINGTON

August 2020

Acknowledgements

I am deeply indebted to Dr. Daejong Kim for helping me overcome many obstacles throughout the course of my graduate studies. This work would not have been possible, without his patience and unwavering support. I would also like to thank Dr. Alan P Bowling and Dr. Bo Wang for obliging to be a part of my thesis defense committee. I would also like to acknowledge the financial support provided by Dr. Daejong Kim and the Department of Mechanical and Aerospace Engineering, University of Texas at Arlington.

Special thanks are due to all the people that have enriched my life by showing me the power of rational thought. The debates and discussions with my friends, colleagues and family have helped me grow intellectually and emotionally.

Finally, I would like to thank my family for the endless love, emotional support and encouragement and for helping me navigate through tough times with ease.

August 3rd , 2020

Abstract

OPTIMUM DESIGN OF SHIMMED FOIL BEARING CONSIDERING ROTORDYNAMIC STABILITY

VENKATA SAI JYOTHISH ATLURI

The University of Texas at Arlington, 2020

Supervising Professor: Daejong Kim

Air foil bearing technology has made substantial development in the past years and has found its applications in high speed turbomachinery. Yet the rotordynamic instability has still been a persisting issue in the single pad air foil bearings. The single pad bearing can resolve this issue by using large clearance with the shaft but the large clearance requires large impeller tip clearance which is not ideal. Multi pad air foil bearings with non-uniform clearance distribution can be used to improve the rotodynamic stability, but the three pad bearings have inferior load capacities due to the less angular length of each pad. To obtain the superior load capacity of the single pad bearing and the rotordynamic stability of three pad bearings, shimmed bearings are introduced. All the previous papers on the shimmed air foil bearings have considered various parameters of the shims to optimize the design but have not performed the analysis by considering the rotordynamic stability. This paper investigates the effect of design parameters of the shim, such as angular span and angular position, on the stiffness and damping characteristics of the bearing. The obtained stiffness and damping characteristics of the single pad shimmed air foil bearing are compared with those of three-pad bearing and the advantages of using a shimmed bearing are discussed. A methodology to optimize the design parameters of the shim to improve the rotordynamic stability of the bearing is shown. Optimized shim parameters are found for a 70mm bearing which is used in 150kW turbo blowers.

Table of Contents

List of Illustrations

List of Tables

Chapter 1 : INTRODUCTION

Bearings are devices that are used to support rotating components in a system. Foil bearings in specific are being used in small high-speed turbo machinery systems in recent years because of its of working principle and advantages. This bearing supports the rotating elements in turbo machinery systems by fluid pressure generated between the rotating element and housing. This pressurization can be caused through two ways either hydrostatic or hydrodynamic mode. In the hydrodynamic mode, the hydrodynamic pressure is produced by the relative motion between the rotor and the top foil of the bearing. The commonly used fluid in these bearings is air, though various other gasses can also be used based on system applications.

Air Foil Bearing Construction

A simple foil bearing is made of two main layers, a top foil with good surface finish and corrugated bump foil. The top foil supports the rotating journal when the whole system is in rest. This top foil is supported by the corrugated foil from underneath. A slight offset known as eccentricity is formed in the bearing because of the shaft weight or any external load. This offset is required for the initial generation of hydrodynamic air film. The two foils, top foil and bump foil are welded to the bearing sleeve to keep them from rotating with the journal. The welded part of the top foil is called trailing edge and the free end is called leading edge. The stiffness and damping coefficient of the bearing is varied by modifying the geometry and

material of the bumps in the bump foil. The foil bearings are also made with tight tolerances in the design and assembly process, this prevents any excessive movement of the shaft preventing the whole system from major failures. The surface of the top foil is coated with solid lubricants to withstand the initial friction from the shaft, this layer also prevents the top foil from early wear.

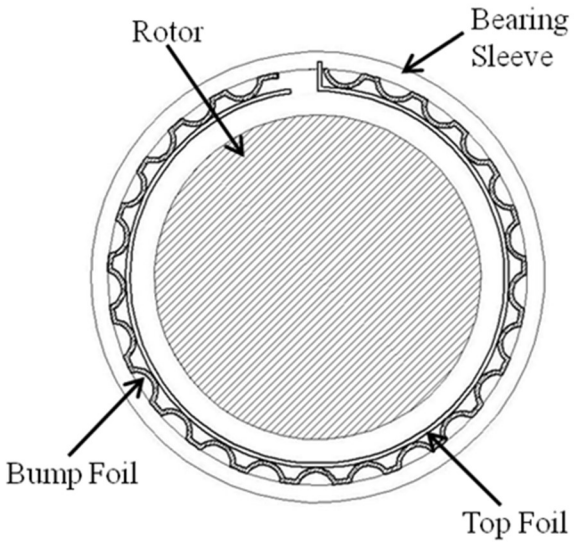

Figure 1 Typical view of single pad foil bearing

Advantages of Foil Bearing

1. Air foil bearings are highly reliable because of its contactless working and the absence of oil pressurization system.
2. Air foil bearings can be used at a wide range of temperatures because the fluid retains its properties throughout the process.
3. Because there is no bulky oil pressurization system the bearing configuration is small and light which can be handy in aerospace applications.
4. Air foil bearings can be used at very high speeds without compromising the efficiency when compared to other bearings.

Disadvantages of Foil Bearing

1. Lower load capacity than the roller or oil bearings.
2. Wear during the start-up and stopping cycles.
3. Self-excited vibration can appear past a given speed, because of the cross coupled stiffness and low damping of gas lubrication.
4. Tight manufacturing tolerances are required, in order to carry sufficient load and avoid the instability mentioned above.
5. The environment surrounding the bearing must be clean because of their small clearances, air foil bearings are sensitive to particulates and dust in the environment.

Working Principle of the Foil bearing

In air foil bearings, a certain amount of pressure must be developed between the shaft and bearing surface to have a smooth and friction less rotation. This pressure is created by a phenomenon called wedging effect. When the whole system is stationary, the shaft centre and the bearing centre are slightly offset due to the shaft weight or external force. The offset is called as eccentricity and the offset is responsible for the wedging effect because it creates a convergent-divergent region for the fluid film. When the shaft is building up the speed, the fluid is drawn into the convergent-divergent region. This convergence causes the clearance to decrease and the pressure increases, this helps to lift off the shaft. The load that can be supported depends on the relative surface speed, the area of the converging region, the shape of the clearance space between the rotating surface and top foil. It also depends on the support structure stiffness and viscosity of the lubricant. The compliance of the bump foil helps when there is any thermal deformation or when there are any vibrations in the journal at high speed or temperatures.

Chapter 2 : LITERATURE REVIEW OF FOIL BEARINGS

This section consists of all the vital research, advancements, and the history of air foil bearings. Agrawal[1] has given a lucid idea of why the foil bearings are used, and the history of foil bearing. Air foil bearings are being used in more and more applications because of their higher reliability, less to no maintenance requirement, high speed operation in extreme temperatures. In a journal bearing the clearance between the shaft and the bearing is very small. The small clearance does not accommodate for the thermal expansion of the shaft or any vibrations caused by the shaft at high temperatures and speeds, respectively. In addition, damping characteristics are required to supress the any whirl instability. To solve these issues foil bearings are introduced. When a shaft grows the foils are pushed further towards the sleeve because of its compliant structure keeping the film clearance relatively unchanged. In addition, the bump foil in a foil bearing provides damping due to relative sliding to suppress the whirl instability. To achieve these characteristics, foil bearings must be designed meticulously by optimising every parameter of the bearing.

In the initial stages of development of the foil bearings, researchers have tried to optimise the geometry of the bump foil to improve the performance of the bearing. Heshmat and Ku[2] have developed a computer program that determines the stiffness, deflection, displacement and reacting forces of each bump taking into consideration the friction between top foil , bump foil and the housing sleeve. The

above described computer program also takes into consideration the local interactive forces between the bumps which can affect the stiffness of the bump foil considerably. This analysis is also done to determine the ideal geometry for the bump foil. The behaviour of the bump stiffness with respect to the bump geometry is given in Figure 2. However, the bump stiffness calculation cannot be calculated by using the friction coefficients as external forces because, friction coefficients are the result of movement of the bumps. Hence the dynamic friction coefficients

cannot be used in a static analysis. The additional resistance to the bump motion is due to the kinetic friction effect within the bump impedance.

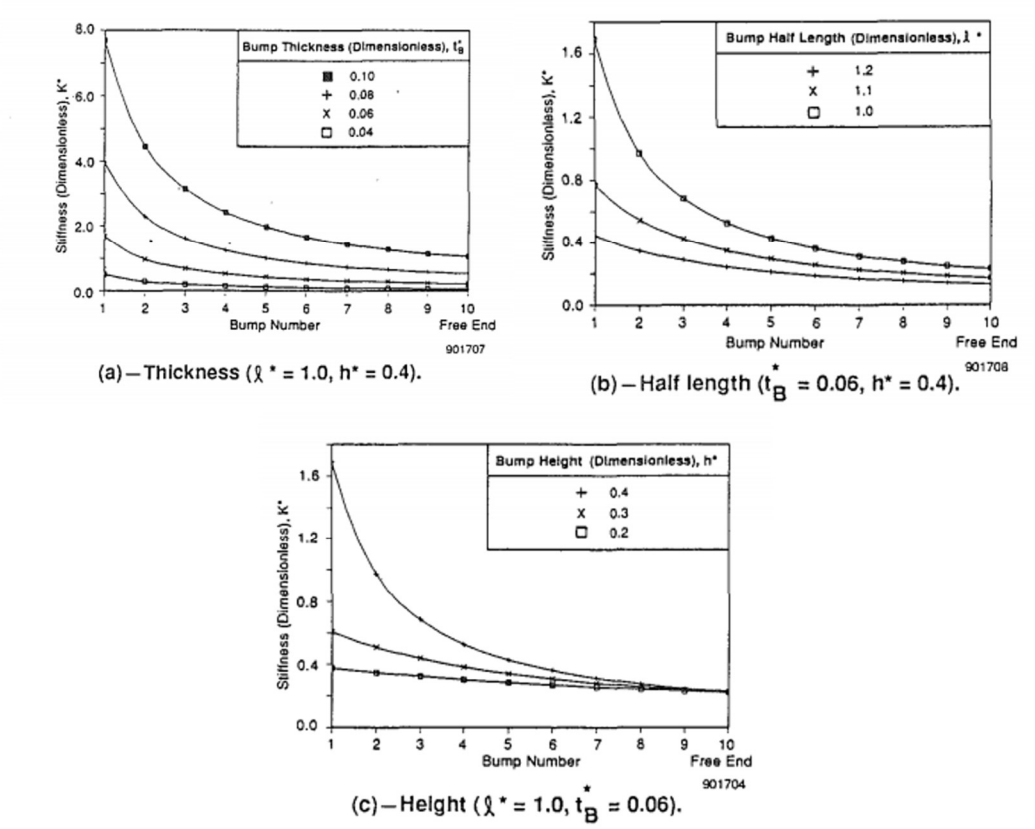

Figure 2 Variation of Bump Stiffness with change in bump geometry from[2].

To further improve the stability of the bearing, most important parameters that affect the stiffness and damping are the attitude angle and eccentricity. To further develop the foil bearings and in order to reduce the friction during the start stop cycles and for thermal management researchers have introduced hydrostatic injection through orifices creates in the bearing. Hydrostatic injection is used to

prevent the friction and reduce the operating temperatures at high speeds. But in recent years, Yazdi and Kim[3] has showed that the controlled injection of the pressurized air can be used to control the rotor position inside the bearing in order to achieve small attitude angle and large eccentricity. The author used the controlled injection as an external force on the rotor to improve stability. Waterfall plots from experimental measurement shows that the onset of sub synchronous vibration is delayed when all the orifices are open, and it is further delayed when the opening of orifices is controlled by closing the bottom orifice and keeping the two top orifices open. For the in phase and out phase imbalance, the synchronous imbalance response was plotted from peak to peak, and the result show that the hybrid air foil bearing system has highest maximum operating speed. Also, with controlled hybrid mode case the amplitude of vibration at critical speeds is less compared to the other two modes. It has been confirmed from both the experimental and numerical analysis that the onset of synchronous vibration is delayed, and the maximum speed of the rotor is also increased from 27k rpm to 45k rpm and the amplitude of

synchronous vibration at critical speed is reduced significantly. Therefore, a significant enhancement in stability is seen while using the hybrid mode.

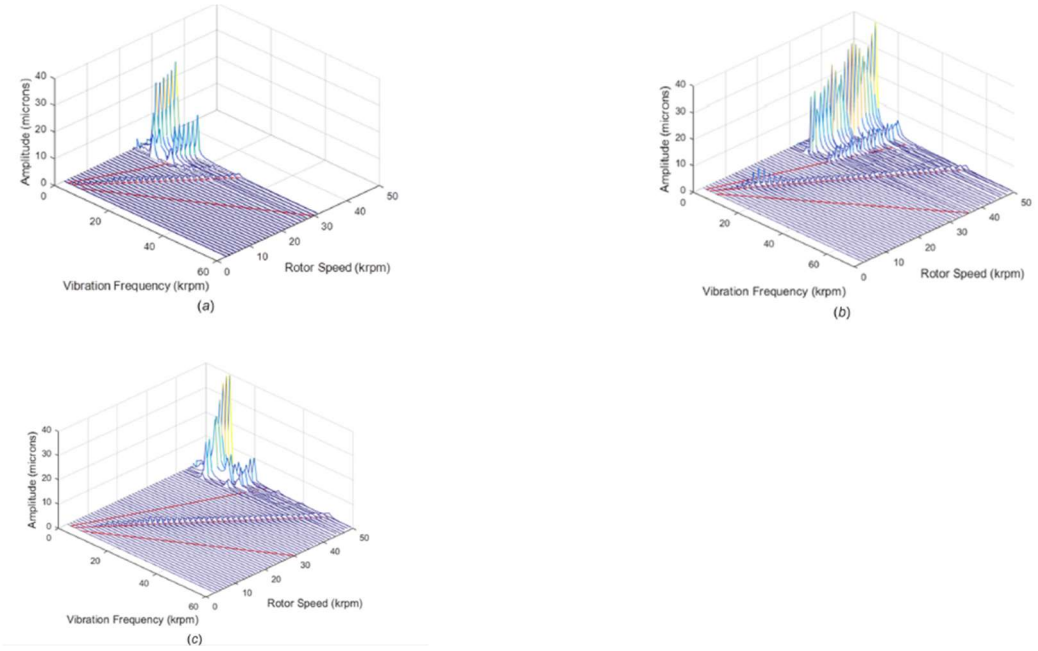

Figure 3 Simulated water fall plots adopted from[3]: (a) hydrodynamic mode, (b) full hybrid mode(when all the orifice are open, (c) controlled injection (when one orifice is closed)

Further analysis into the controlled hybrid injection system has yielded some interesting results. A study by Yazdi and Kim [4] has shown that the controlled injection of pressurized air to a single pad hybrid air foil bearing can increase the onset speed of sub synchronous vibration. The authors have achieved this effect by varying the location of the injection points. Three different cases with three

different orifice location configurations are compared to find the optimum layout. The configurations are given in Table 1.

Table 1 Angular Orifice locations adopted from [4].

Case Number	1st orifice Location	2nd orifice Location	3rd orifice Location
Case 1	30	180	330
Case 2	60	180	300
Case 3	90	180	270

After performing orbit simulation to predict the imbalance response the authors have concluded that case 1 has highest rotordynamic stability while case 3 has the lowest rotordynamic stability. Predicted rotor eccentricity and attitude angle show that case 1 has highest eccentricity and case 3 has the lowest eccentricity. Frequency domain analyses at 40krpm show that case 2 and case 3 have negative damping at frequency ratios below 0.35. For case 1 it has positive damping for the entire frequency ratio range. In combination large eccentricity paired with positive damping yields better rotordynamic stability.

To improve the stability characteristics of the bearing using a different approach without using the hydrostatic pressure, the basic operating fundamentals that are unique to the bearing must be studied. To nurture the development of foil bearings, researchers have performed simulation and experimentation by varying radial

clearance that affect the performance of air foil bearings. Radil [5] showed the effect of varying clearance on the load capacity coefficients of foil bearings by doing a parametric study on two bearings with different initial clearances. The load capacity is found by running the rotor 30000 rpm and gradually increasing the load on the rotor until the rotor exhibiting dramatic increase in torque and decrease in speed. These two symptoms are the signs of rubbing contact. In the experiments the clearance is gradually increased by incrementally reducing the diameter of the mating journal using an in-place grinding system. The change of the load capacity

coefficient with the varying radial clearance is given in Figure 4. The load capacity coefficient in paper [5] is defined as following,

$$\mathrm{I} = \frac{W}{LD^2\Omega} \tag{1}$$

Where, W is maximum steady state load that can be supported, N

L is the bearing axial length

D is the shaft diameter

Ω is the shaft speed.

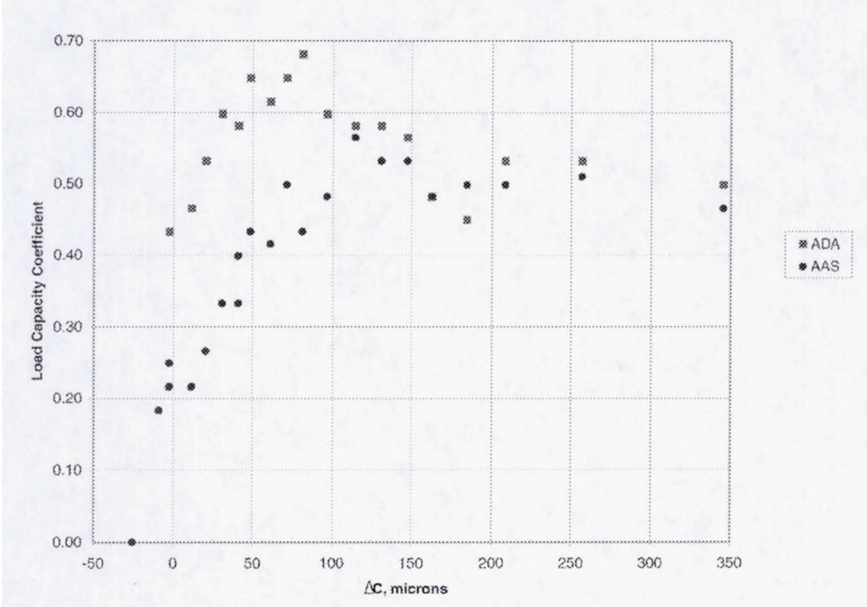

Figure 4 Variation of load capacity coefficient of the two test bearings plotted as a function of radial clearance, adopted from [5]

According to Radil [5] it can be concluded that the load capacity and the stability characteristics can be improved by increasing the radial clearance of the bearing. However due to the increased radial clearance in the bearing a large impeller tip clearance is created. Joost [6] has studied the overall performance of the compressor by changing the impeller tip clearance. He has found that there was a significant output head and pressure output decrement with the increase in impeller tip clearance. Hence single pad bearings with large clearances cannot be used.

In general, when a fixed wall geometry journal bearing is considered, to improve the stability of the bearing, researchers performed experiments on bearings with various bearing geometries. One of the experimentally proven solutions for improving the stability of bearing is by creating a pressure dam as presented by Leader [7]. Leader [7] has experimentally proved that pressure dam bearings have improved stability characteristics with the optimum pressure dam parameters. Leader [7] performed experimental and spectral analysis on three types of bearings. The three types of bearings are axial groove bearing, pressure dam bearing and a tilting pad bearing. When the instability onset speeds are compared for the three bearings pressure dam bearing and the tilting pad bearing has higher stability threshold speeds. The onset of instability for axial groove bearing is at 5750 rpm. For the pressure dam and tilting pad bearings the instability onset speed is 8400 rpm and 10130 rpm respectively. Further stability analyses are done on the three

bearings to evaluate the amplitude and frequency of the vibration. The water-fall plots show that the axial groove and the pressure dam bearings show much lower vibration amplitude than the tilting pad bearings at critical speeds. Pressure dam bearings show this type of characteristic because of the pressure dam shape in the bearing. To improve the stability of the bearing, the critical mass of the rotor plays a vital role. A range of eccentricity must be maintained as per the bearing requirements. To maintain this eccentricity of the rotor a downward force must be applied on the shaft. To create the downward force on the shaft the fluid film is pressurised. This hydrodynamic pressurisation is done by creating the wedging effect. Wedging effect is created by adding geometries like pressure dams or Rayleigh steps. When shaft starts to rotate the oil is forced into the dam region and hydrodynamic pressure is created on the shaft. This pressure on the shaft increases its eccentricity stabilising the shaft. It can be concluded that better stability

characteristics can be obtained by changing the bearing geometry and creating a variable clearance throughout the bearing.

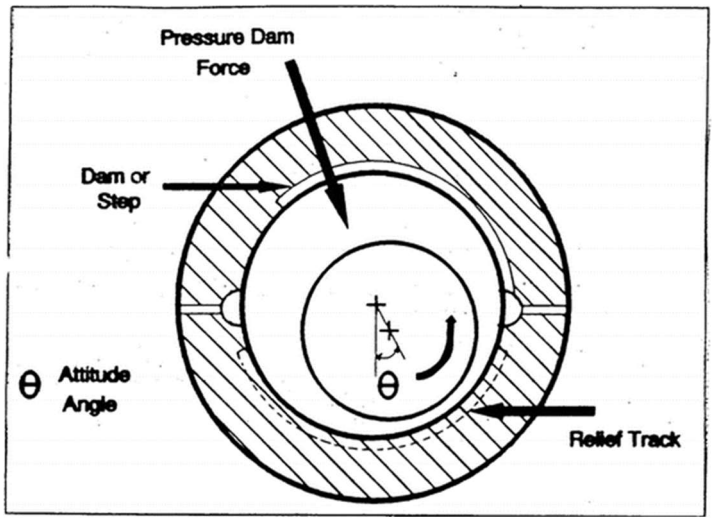

Figure 5 Example of a Pressure Dam Bearing adopted from [8]

To apply the above stated type of approach of variable clearance distribution to the air foil bearings, Kim [9] has first introduced a three pad foil bearing with varying top foil geometry for the first time in 2007. All the previous research done on foil bearings assume that the top foil is circular regardless whether the top foil is continuous or disconnected three pad configurations. Introduction of this bearing has paved the way for many researchers to pursue this approach of varying top foil geometry. The three-pad bearing design is clearly shown in Figure 7 and Figure 8. In Figure 8 θ_{SB} is the angular location of minimum film thickness and θ_{pad} is the angular width of the pad. The preload in the three-pad bearing is shown in Figure 6 which is the distance between bearing centre and the pad center. Kim[9]

investigated the load capacities and rotor dynamic performance of the three-pad bearing and compared it with the circular cylindrical bearing with continuous top foil geometry. Also, to consider the behaviour of bump foil structures stiffness variation along the axial and circumferential directions was incorporated for the two type of bearings. The above characteristics of these bearings are compared by calculating the load capacities, dynamic force coefficients and by performing modal stability analyses and time domain orbit simulations.

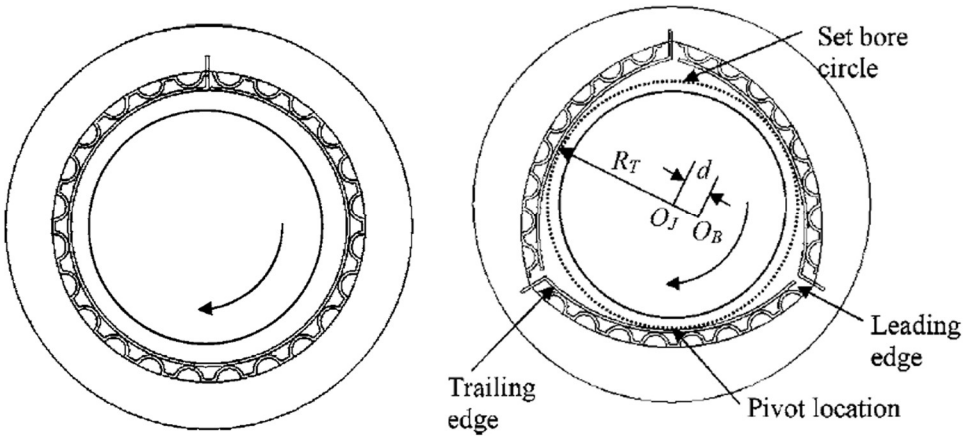

Figure 6 Schematic of the two types of bearing in [9]. Left is a single pad bearing and Right is three-pad bearing.

Kim [9] has concluded that the there is significant decrease in load capcity in the three pad bearings due to the very less angular arc length of 120 degrees for each pad. However when the orbit simulation is done, the onset speed of instability is significantly higher when compared to that of the single pad bearing. The onset speed of three pad bearing is 47000 rpm while the onset speed of the single pad

bearing is 24000rpm. The increease in onset speed shows the rotordynamic stability of the three pad bearing is better than the single pad bearing, but the single pad bearings have better load capacity than that of the three pad bearing.

The figures below show the typical view of a three-pad bearing and the parameters of the bearing. The figures are adopted from [10].

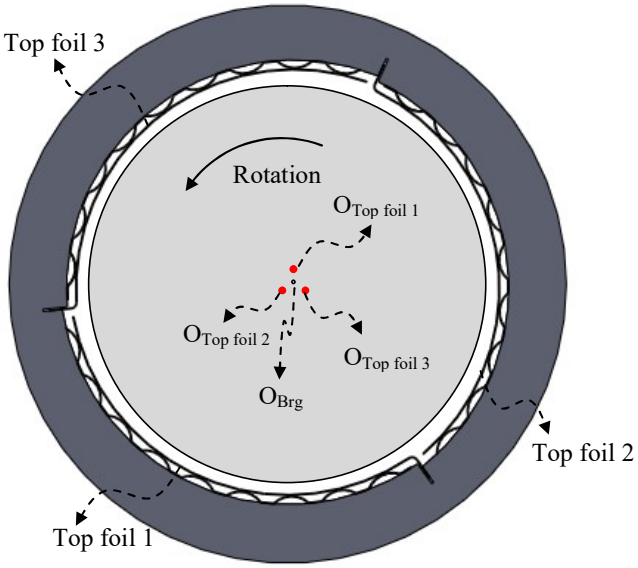

Figure 7 Three pad Foil bearing with the center of curvatures of each pad.

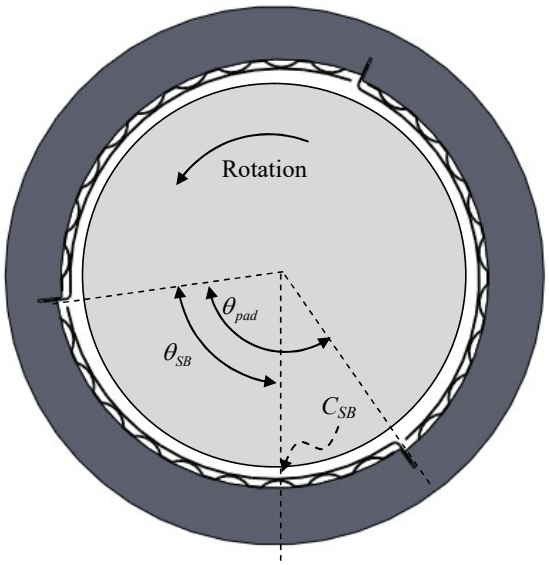

Figure 8 Three pad bearing with the angular span and the angular position of minimum film thickness

Schiffmann and Spakovszky [11] have introduced a concept of selective shimming to improve the foil bearing stability. Selective shimming is a way to manage the dynamic stiffness and damping of the bearing. This method can help in finding the optimum design for a bearing with less instability. The authors have concluded that selective shimming is an effective means to improve the rotordynamic performance and the stability threshold of foil bearing by implementing a rotordynamic model and performing spectral analysis. Selective shimming is done by implementing shims with varying thickness in the design of the bearing. The methodology behind this is to vary the pressure distribution to increase the stability threshold. The critical mass parameter is used to optimise the selective shim distribution for

improving the stability threshold. The stability of the bearing is characterised as a critical mass. Critical mass is the rotor mass that makes the bearing unstable.

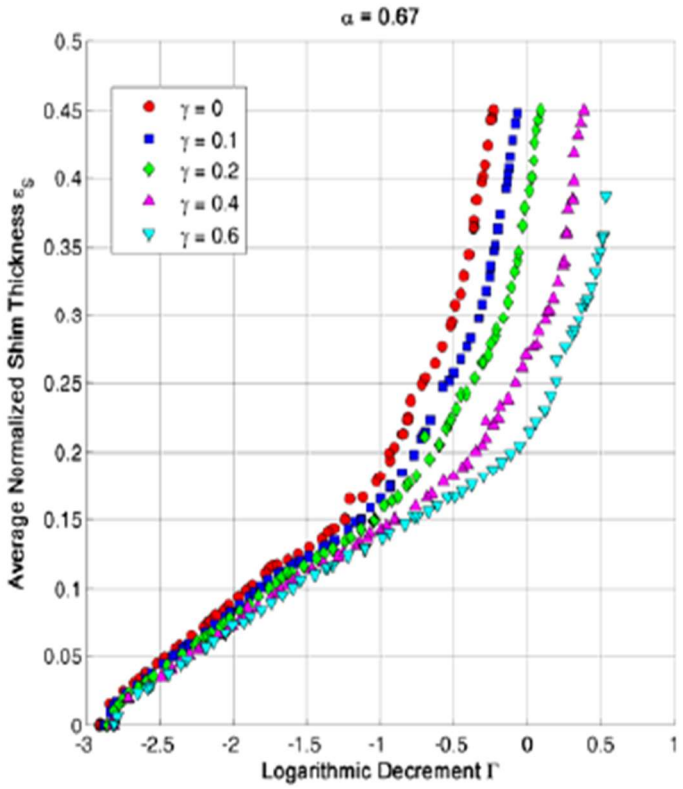

Figure 9 Pareto curves adopted from [11]. X-axis is logarithmic decrement of feed parameter.

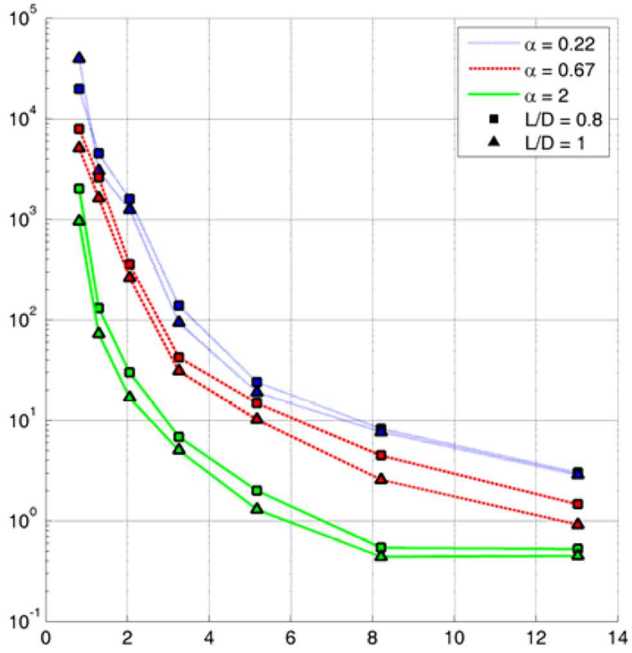

Figure 10 Critical mass variation with respect to the bearing number adopted from [11]. X-axis is compressibility number or bearing number. Y-axis is Critical mass.

Schiffmann and Spakovszky [11] have concluded from the plots that the critical mass parameter can be increased by two orders of magnitude by optimising the shim parameters. They have given some simple guidelines for various configurations of the foil bearing geometries. These configurations are divided for a variety of bearing geometries with different L/D ratio, compliance and bearing number. Figure 10 shows the variation of critical mass for various bearing configurations.

Further on in order to study the effect of shims on the performance of the bearing Hoffmann and Liebich [12] have performed dynamic analysis by varying

static preload, dynamic amplitude and examined the excitation frequency. Further on the authors have evaluated the dynamic stiffness and damping coefficients by varying the position of the shims and static preload. The two shim positions that are evaluated are 90 degrees and 135 degrees as shown in Figure 11. The authors have concluded that with the increase in static preload dynamic stiffness is increased and more damping is generated due to the raised contact forces and more activated bumps. Damping is increased in the 135-degree position shimmed bearing when compared to that of the 90-degree positioned shimmed bearing. The simulation and experimentation in the paper are performed for only to angular positions of the shim with constant angular span.

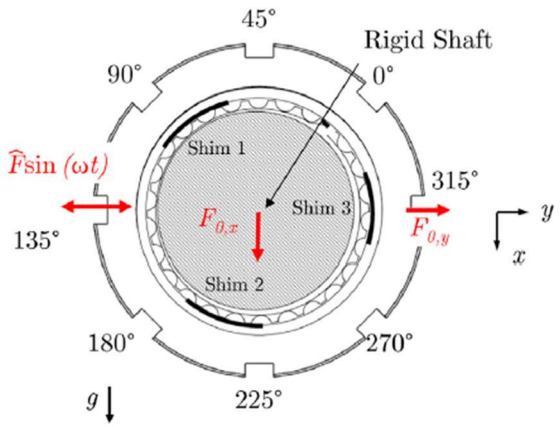

Figure 11 Cross Section of the bearing mounted on a rigid shaft including the acting forces due to preload $F_{0,y}$, horizontal dynamic excitation and gravity force of the bearing.

Research Objective:

As discussed above it has been proved that adding a shim can vary the stability of a bearing considerably. By adding a shim to the single pad bearing all the rotor dynamic advantages of having a large clearance can be obtained and also by restricting the maximum allowable movement of the shaft a much more stable system is formed. The bearing used for this simulation is used in a 150kW turbo blower with a shaft weight of 30kg. So, to determine the ideal design for this specific application, bearing simulation is performed with various shim thickness, shim location and angular span to achieve the best rotordynamic stability. Modal stiffness and damping curves are plotted to determine the ideal shim location, span, and thickness for a specific requirement. The analyses are also with a single pad

foil bearing to determine the ideal parameter of shim, and compared with three-pad bearing.

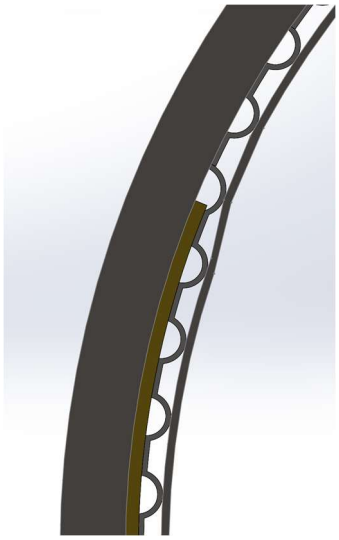

Figure 12 Zoomed in picture a shimmed foil bearing

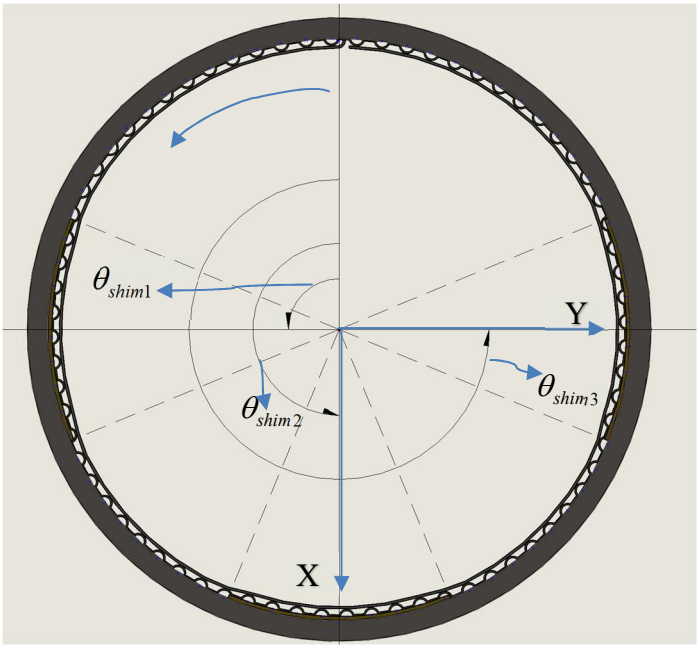

Figure 13 Angular positions of each shim

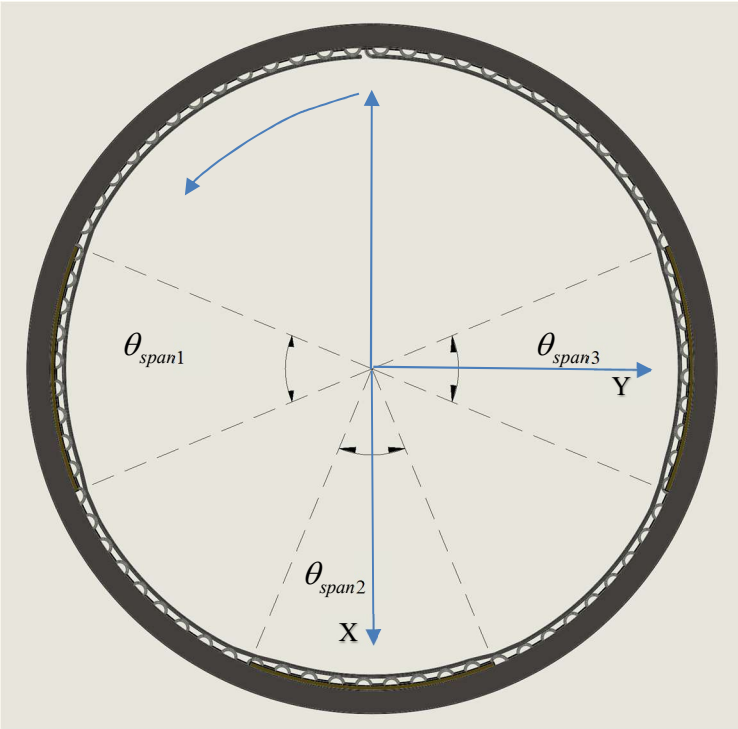

Figure 14 Angular spans of each shim

In the above Figure 13 each angle shows the angular position of each with respect to the YX-axis. In Figure 14 each angle denotes the angular span of each shim.

Chapter 3 : FOIL BEARING DESIGN

Various researchers have been doing extensive research on the analytical and experimental study of a bearing to identify various parameter of a bearing that effect the stability of the bearing. This chapter presents and defines the parameters that are used to change the stability of the bearing. The typical design configuration of the foil bearing is given in Figure 1. Here the top foil functions as a bearing surface and corrugated bump foil serves as elastic foundation supporting the top foil. In this bearing the bearing not only has stiffness but also Coulomb type damping which is caused by the sliding friction. And there is usually no pre-existing preload because of the non-visible clearance.

Assembly Clearance:

Radial clearance is the most important parameter in a bearing that effects the stability of the bearing. In an air foil bearing as the shaft rests on the bearing it can be misunderstood that it has no radial clearance but the clearance in this bearing is measured in a different way. The shaft movement radially inside the bearing can be told as the clearance of the bearing. This shaft movement is possible because of the small gaps between the bump foil and top foil and the bump foil and bearing sleeve. These gaps are called as play or looseness by some researchers. The procedure for determining this radial clearance is given by [5]. Radil [5] uses a load-displacement curve to determine this clearance. This change in radial clearance affect the load capacity coefficients which in turn affects the limits of the bearing's stability. To

change this radial clearance in the bearing in this paper the shims are introduced. This makes it easy to tailor the radial clearance to the user's needs.

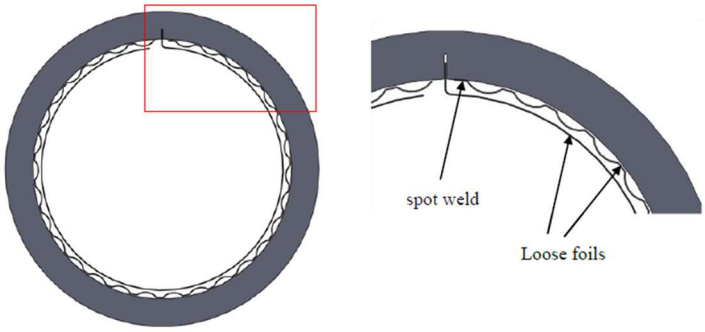

Figure 15 Exaggerated foil assembly condition before assembly onto the rotor.

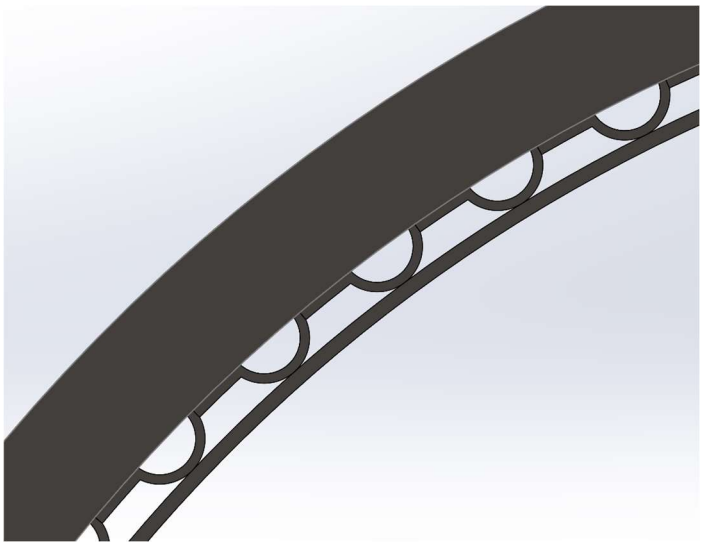

Figure 16 Zoomed in picture of a solid model of Foil Bearing

The total bearing clearance at normal operating condition (at high hydrodynamic pressure) is always the summation of the assembly clearance and bump deflection. Therefore, the bearing clearance can be given as,

$$h(z,\theta) = C(\theta) + e_x \cos\theta + e_y \sin\theta + \delta(z,\theta) \tag{2}$$

where $\delta(z,\theta)$ is the deflection of the bump, and (e_x, e_y) are the cartesian coordinates of the rotor center with respect to the bearing center.

Chapter 4 : MODELLING OF THE BEARING

This chapter covers the mathematical modelling for the simulation. All the formulations in this chapter are based on the formulations presented in Kim [9]. To evaluate the dynamic performance of the foil bearing, the bearing stiffness and damping coefficients must be found. Perturbation method is used to calculate these coefficients dependant on the excitation frequency as well as operating speed. Furthermore, modal analysis is performed to find the impedance of the bearing; modal stiffness and modal damping. To use the perturbation method, static equilibrium point must be found first. Static equilibrium point is where the rotor weight and external load is balanced by the bearing reaction. In the perturbation analysis, a small disturbance of $\Delta e_x, \Delta e_y$ amplitude and frequency of ω_s is added to the rotor which is in static equilibrium. Reynolds equation is used to model the air film in the bearing and find the reaction forces of the bump foil bearing. The

Reynolds equation is derived using the continuity and momentum equation with assumptions of negligible inertia, thin film, incompressible flow, and ideal gas.

Eq. (3) show the non-dimensionalized Reynolds equation using $P = \frac{p}{p_a}$,

$H = \frac{h}{C}, \varepsilon = \frac{e}{C}, \nu = \frac{\omega}{\omega_s}$ and $\tau = \omega t$.

$$\frac{\partial}{\partial\theta}(PH^3\frac{\partial P}{\partial\theta}) + \frac{\partial}{\partial Z}(PH^3\frac{\partial P}{\partial Z}) = \Lambda\frac{\partial}{\partial\theta}(PH) + 2\Lambda\nu\frac{\partial}{\partial\tau}(PH) \tag{3}$$

where, ω_s is the excitation frequency and ω is the rotational speed.

The non-dimensional pressure, film thickness, and bump deflection would become

$$P = P_0 + \Delta P = P_0 + \Delta\varepsilon_X P_X e^{i\nu\tau} + \Delta\varepsilon_Y P_Y e^{i\nu\tau} \tag{4}$$

$$H = H_0 + \Delta H = H_0 + \Delta H_X e^{i\nu\tau} + \Delta H_Y e^{i\nu\tau} \tag{5}$$

$$U = U_0 + \Delta U_X e^{i\nu\tau} + \Delta U_Y e^{i\nu\tau} \tag{6}$$

where,

$$\begin{aligned} \Delta H_X &= \Delta\varepsilon_X \cos\theta + \Delta U_X \\ \Delta H_Y &= \Delta\varepsilon_Y \sin\theta + \Delta U_Y \end{aligned} \tag{7}$$

ΔU_x is the non-dimensional deflection of bump due to Δe_x .Similar meaning for ΔU_y .

MODELLING OF THE BUMPS IN THE BUMP FOIL BEARING:

The motion of the bumps is very complex. When force is applied on the bumps, bumps undergo circular stretching motion with dry friction with top foil and sleeve.

For perturbation analysis, the bumps are modelled as a series of inertia-less linear spring damper, as shown in Eq. (8);

$$f_b = k_b u + c_b \frac{du}{dt} \tag{8}$$

f_b is the force caused by the pressure on the bump given by $f_b = \left(p - p_b \right) A_0$, where A_0 is an effective area that the bump covers. k_b is the bump stiffness and c_b is the equivalent bump viscous damping coefficient.

The equivalent bump viscous damping coefficient is found from equivalence of dissipated energies during one cycle of motions under viscous damping and dry frictional damping. The relation for the viscous damping can be given by,

$$c_b = \eta \frac{k_b}{\omega_s} \tag{9}$$

The structural loss factor η of bumps is measured by load deflection tests with a dummy shaft slightly larger than actual journal shaft to have zero clearance. This loss factor ranges from 0.1 to 0.3 depending upon the bump design. Perturbation is

also applied to Eq. (8) to eliminate ΔU_x and ΔU_y in Eq. (7), and further details can be found in Kim [9].

The final form of the first order Reynolds Equation is,

$$\begin{aligned}
&\frac{\partial}{\partial\theta}\left[\Lambda H_0 P_\alpha - P_0 {H_0}^3 \frac{\partial P_\alpha}{\partial\theta}\right] + \frac{\partial}{\partial Z}\left[-P_0 {H_0}^3 \frac{\partial P_\alpha}{\partial Z}\right] \\
&= \frac{\partial}{\partial\theta}\left[{H_0}^3 \frac{\partial P_0}{\partial\theta} P_\alpha - \Lambda P_0\left(\frac{P_\alpha}{K_b(1+\eta i)} + h_\alpha\right) + 3{H_0}^2 P_0\left(\frac{P_\alpha}{K_b(1+\eta i)} + h_\alpha\right)\frac{\partial P_0}{\partial\theta}\right] \\
&+ \frac{\partial}{\partial Z}\left[{H_0}^3 \frac{\partial P_0}{\partial Z} P_\alpha + 3{H_0}^2 P_0\left(\frac{P_\alpha}{K_b(1+\eta i)} + h_\alpha\right)\frac{\partial P_0}{\partial Z}\right] \\
&-2\Lambda\nu i\left(P_0\left(\frac{P_\alpha}{K_b(1+\eta i)} + h_\alpha\right) + P_\alpha H_0\right)
\end{aligned} \tag{10}$$

where, α=X,Y and $h_x = \cos\theta$ and $h_y = \sin\theta$

Once the first order Reynolds Equation is solved, the stiffness and damping coefficients are calculated using the equations given below.

$$\begin{pmatrix} k_{XX} \\ k_{YX} \end{pmatrix} = -\frac{W_0}{C}\frac{R}{2L}\iint \mathrm{Re}(P_x)\begin{pmatrix}\cos\theta \\ \sin\theta\end{pmatrix} d\theta dZ = \frac{W_0}{C}\begin{pmatrix} K_{XX} \\ K_{YX}\end{pmatrix} \tag{11}$$

$$\begin{pmatrix} k_{XY} \\ k_{YY} \end{pmatrix} = -\frac{W_0}{C}\frac{R}{2L}\iint \mathrm{Re}(P_Y)\begin{pmatrix}\cos\theta \\ \sin\theta\end{pmatrix} d\theta dZ = \frac{W_0}{C}\begin{pmatrix} K_{XY} \\ K_{YY}\end{pmatrix} \tag{12}$$

$$\begin{pmatrix} d_{XX} \\ d_{YX} \end{pmatrix} = -\frac{1}{\omega_s}\frac{W_0}{C}\frac{R}{2L}\iint \mathrm{Im}(P_x)\begin{pmatrix}\cos\theta \\ \sin\theta\end{pmatrix} d\theta dZ = \frac{1}{\omega_s}\frac{W_0}{C}\begin{pmatrix} D_{XX} \\ D_{YX}\end{pmatrix} \tag{13}$$

$$\begin{pmatrix} d_{XY} \\ d_{YY} \end{pmatrix} = -\frac{1}{\omega_s}\frac{W_0}{C}\frac{R}{2L}\iint \mathrm{Im}(P_Y)\begin{pmatrix}\cos\theta \\ \sin\theta\end{pmatrix} d\theta dZ = \frac{1}{\omega_s}\frac{W_0}{C}\begin{pmatrix} D_{XY} \\ D_{YY}\end{pmatrix} \tag{14}$$

Once stiffness and damping coefficients are calculated, the bearing impedances can be defined as,

$$\begin{aligned} Z_{XX} &= k_{XX} + jd_{XX}\omega_S \\ Z_{YX} &= k_{YX} + jd_{YX}\omega_S \\ Z_{XY} &= k_{XY} + jd_{XY}\omega_S \\ Z_{YY} &= k_{YY} + jd_{YY}\omega_S \end{aligned} \tag{15}$$

From these direct and cross coupled impedances, modal impedances are calculated along the forward and backward shaft whirling motions through 2 DOF eigen value analysis. Details of the eigen value analysis is presented in Ref [9].In this thesis, only forward impedance is considered because imbalance excitation causes only forward whirl. The backward whirl can be excited when shaft rubs against any stationary components such as seals nearby the bearing. However, the modal damping for the backward whirl is always large positive because the backward whirl is against the fluid motion. . Hence backward whirl is not of interest. The formula for forward impedance is given below.

$$Z_f = \frac{Z_{XX} + Z_{YY}}{2} - \sqrt{\left(\frac{Z_{XX} + Z_{YY}}{2}\right)^2 - \left(Z_{XX}Z_{YY} - Z_{XY}Z_{YX}\right)} \tag{16}$$

The real part of Z_f is modal stiffness and imaginary part of Z_f is modal damping.

Chapter 5 : RESULTS AND DISCUSSION

The simulations are performed varying the angular span and location of the shims and the results are compared with that of the single pad bearing and three-pad bearing. . The bearing used in the simulation is used in a 150kW turbo blower with a rotor mass of 7.5kg. Bearing parameters used for the simulation are given below,

Table 2 Basic Bearing Parameters for Shimmed Bearing

Bearing Parameter	Value	Units
Diameter of the bearing	70	mm
Length of the bearing	70	mm
Number of bumps	72	
Top Foil Thickness	203	μm
Shim Thickness	100	μm
Nominal Clearance	248	μm
Bump Foil Stiffness	10	MN/m

Table 3 Single Pad Bearing Parameters

Bearing Parameter	Value	Units
Diameter of the Bearing	70	mm
Length of the Bearing	70	mm
Nominal Clearance	148	mm

Effect of Shim Angular Position

The simulations are performed by changing various shims parameters, and the results are presented below. The angular positions of the shims impact the stability of the bearing, and this can cause lower stability of the bearing when the shims are placed at wrong locations. . Here each simulation is performed by varying the frequency ratio $\nu = \frac{\omega_s}{\omega}$, where ω_s is the excitation frequency and ω is the rotor speed. The frequency ratio is varied from 0.05 to 3. Four shim locations and the angular span varying from 25 to 45 degrees are used as shown in Table 4. The performance of the bearing is judged by evaluating the direct and cross coupled stiffness and damping coefficients, and stability characteristics through plotting forward modal impedance.

Table 4 Angular locations of the shims with shim angular span of 45°

Case No:	Location of shim 1	Location of shim 2	Location of shim 3
1	90	180	270
2	60	180	300
3	30	180	330
4	120	180	240

The reference coordinate for the locations and span of the shims are shown in Figure 13.

The stiffness and damping curves for Case 1~Case 4 are given in Figure 17~ Figure 24.

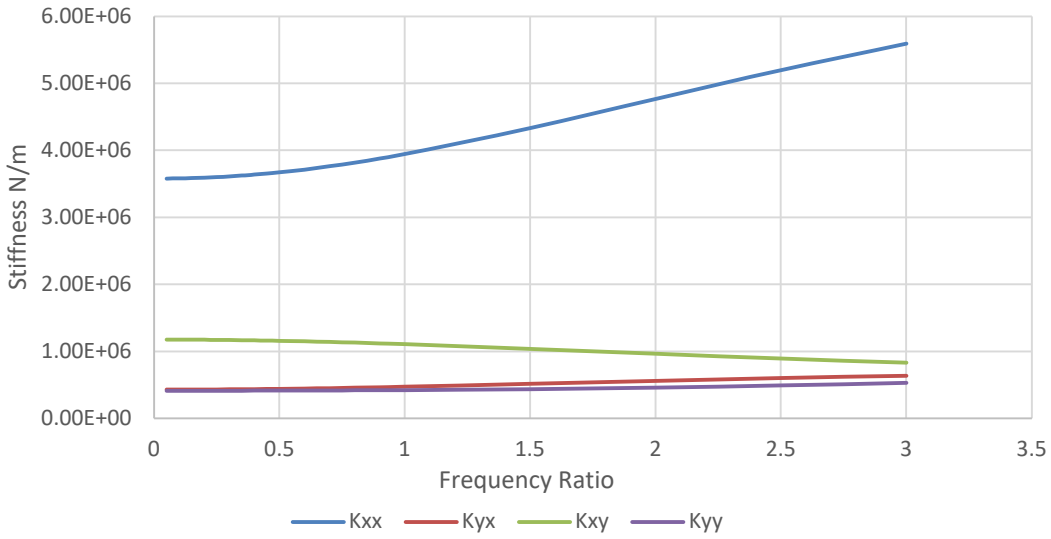

Figure 17 Stiffness coefficients for Case 1 as a function of excitation frequency ratio at 36krpm

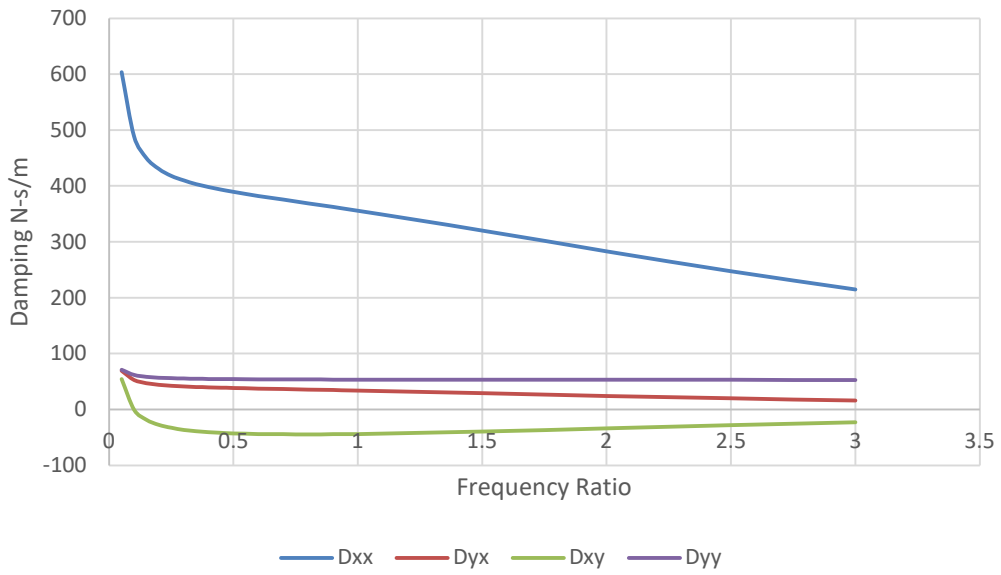

Figure 18 Damping coefficients for Case 1 as function of excitation frequency ratio at 36krpm

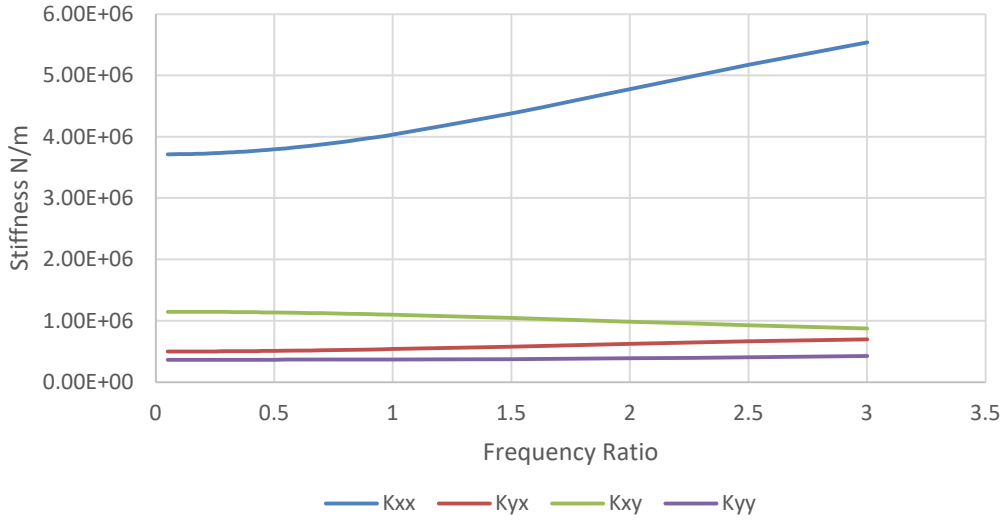

Figure 19 Stiffness coefficients for Case 2 as a function of excitation frequency ratio at 36krpm

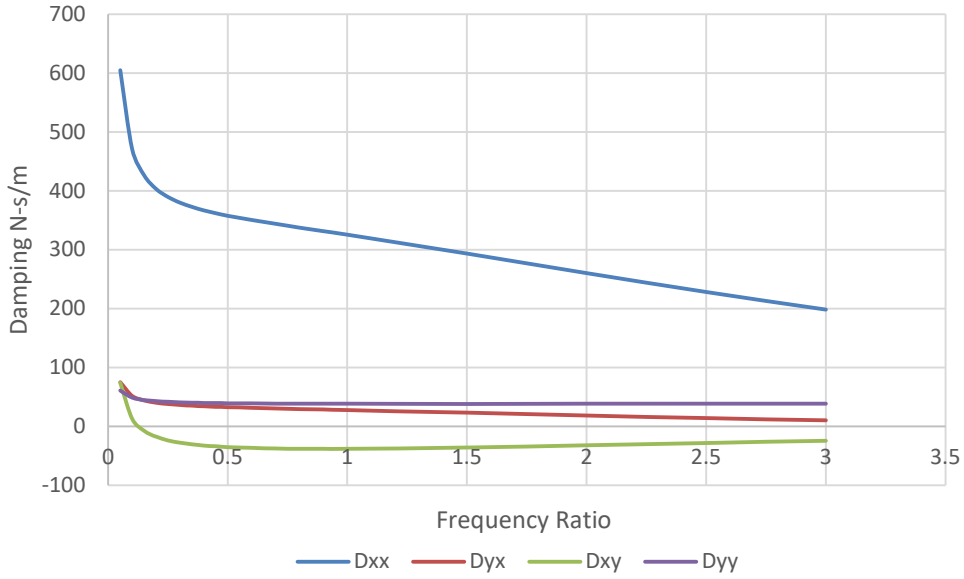

Figure 20 Damping coefficients for Case 2 as a function of excitation frequency ratio at 36krpm

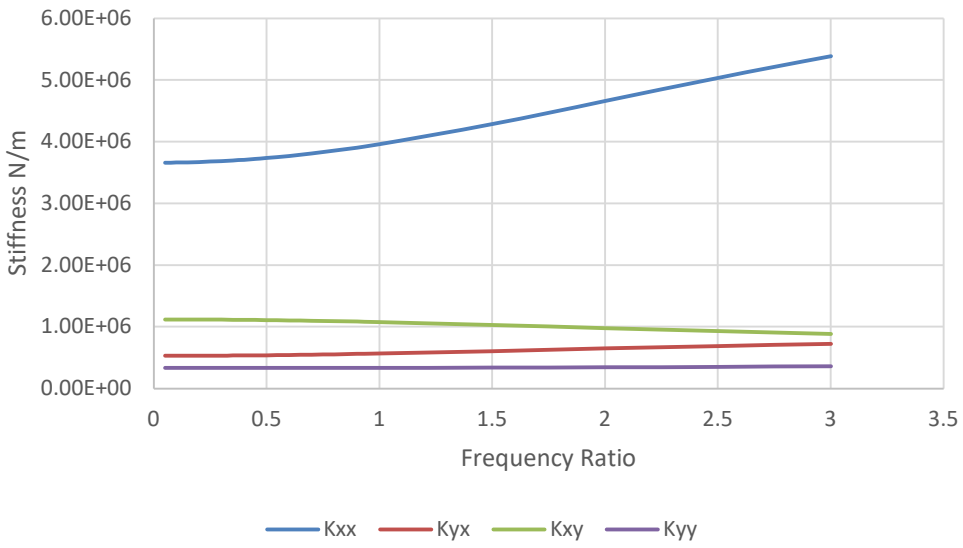

Figure 21 Stiffness coefficients for Case 3 as a function of excitation frequency ratio at 36krpm

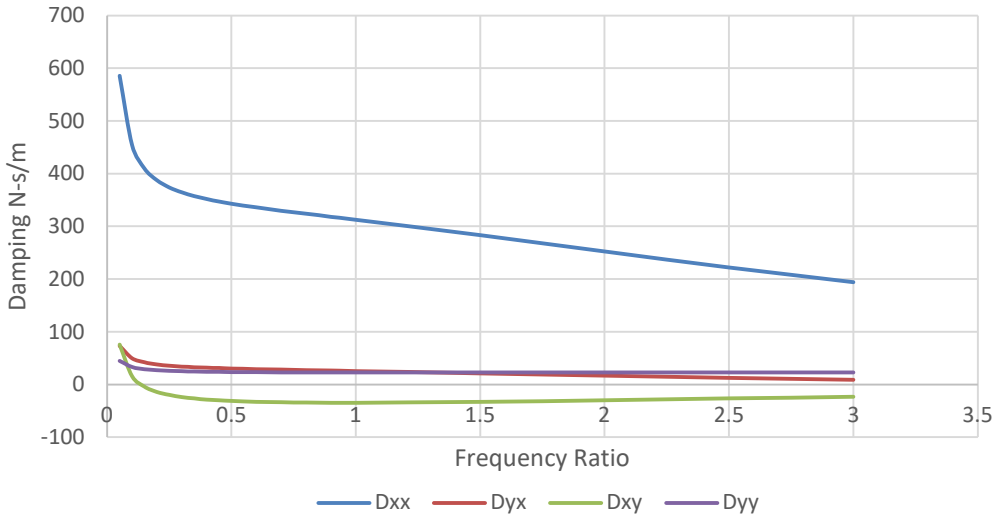

Figure 22 Damping coefficients for Case 3 as a function of excitation frequency ratio at 36krpm

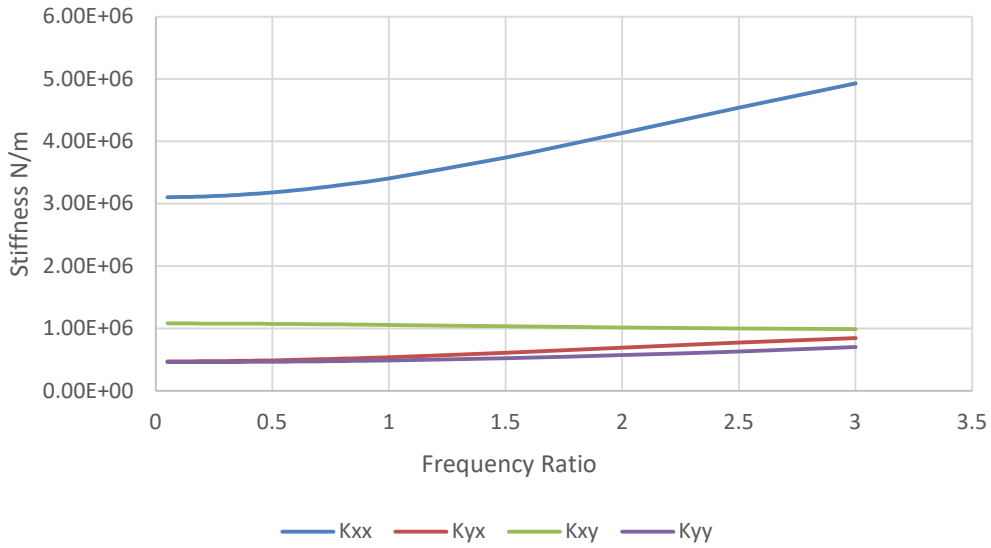

Figure 23 Stiffness coefficients for Case 4 as a function of excitation frequency ratio at 36krpm

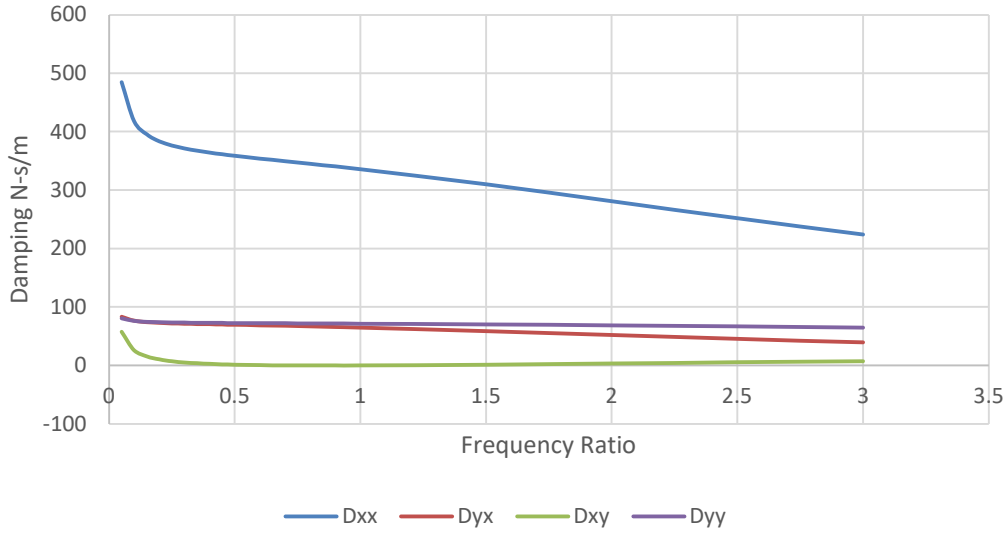

Figure 24 Damping coefficients for Case 4 as a function of excitation frequency ratio at 36krpm

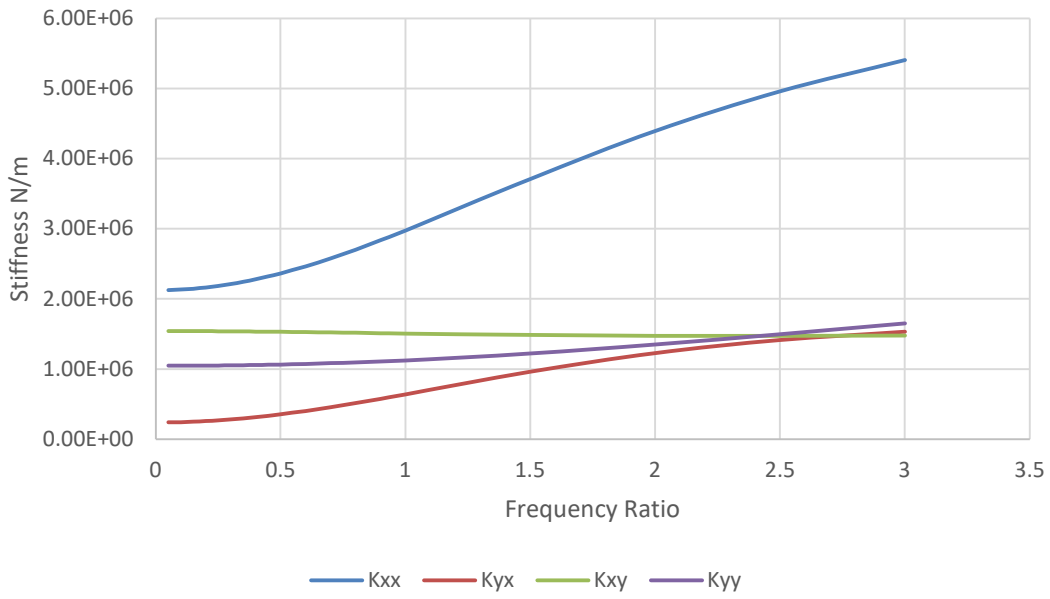

Figure 25 Stiffness coefficients for single pad bearing as a function of excitation frequency ratio at 36krpm

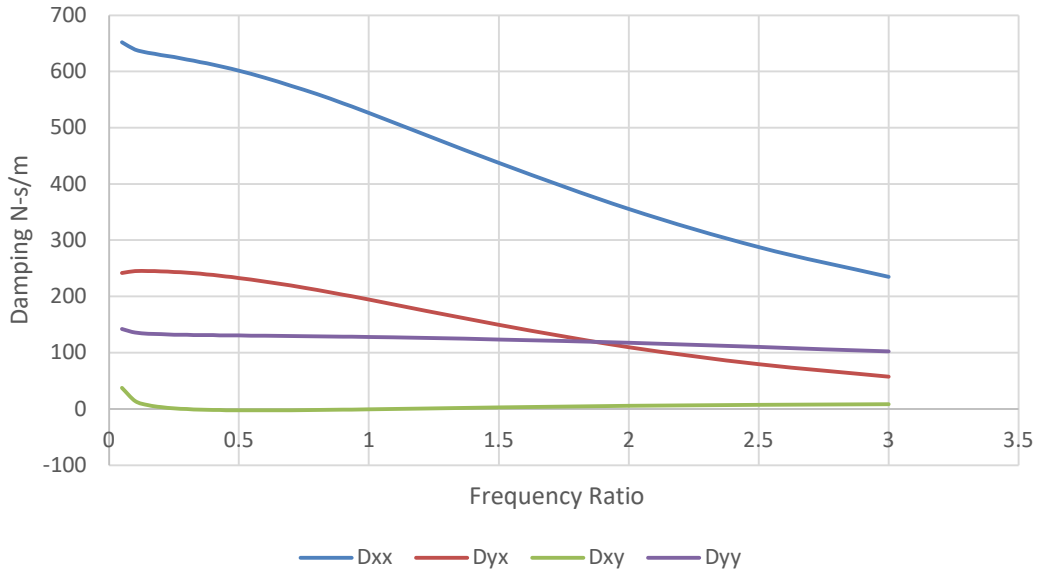

Figure 26 Damping coefficinets for single pad bearing as funmction of excitation frequency ratio at 36krpm

All the cases have a similar behaviour of stiffness and damping with the maximum and minimum values changing. To get a much more in-depth understanding of stability characteristics of each case, the combined effect of all the stiffness and damping coefficients must be studied through modal stiffness and modal damping, which are obtained from the modal impedance.

Figure 27~Figure 30 present modal impedance of the each case shown in Table 4.

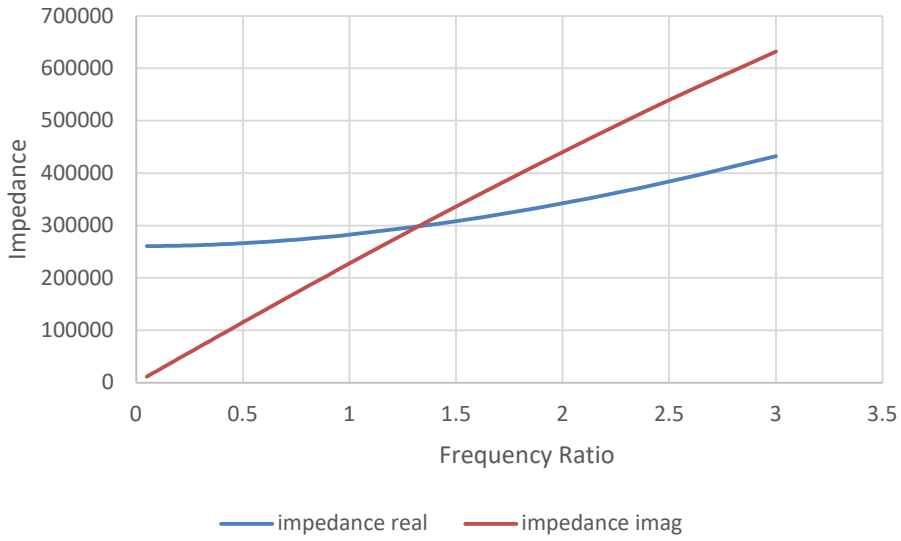

Figure 27 Impedance curves of Case 1

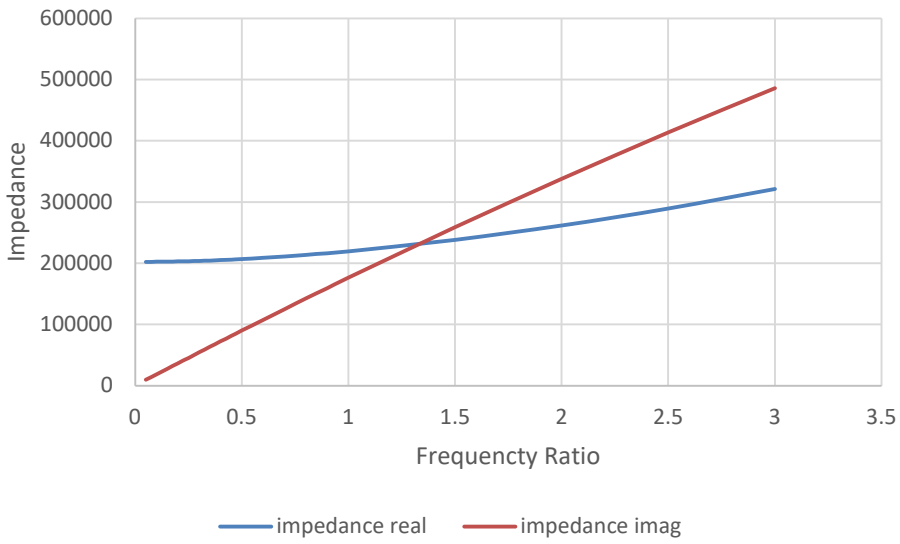

Figure 28 Impedance Curves of Case 2

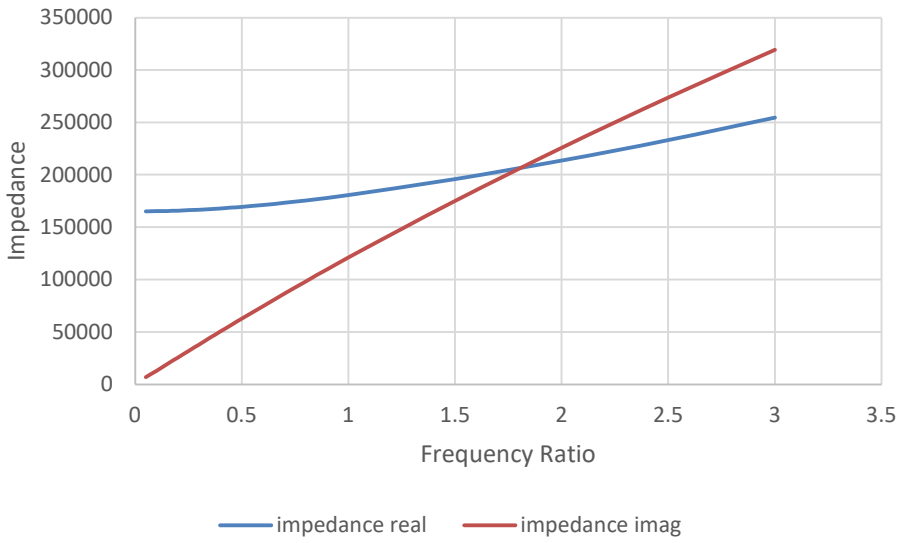

Figure 29 Impedance Curves of Case 3.

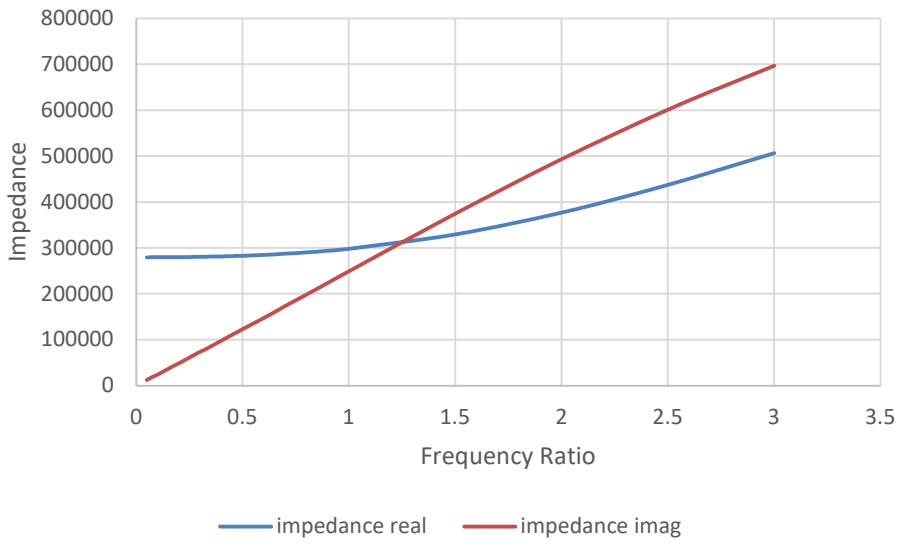

Figure 30 Impedance curves of Case 4.

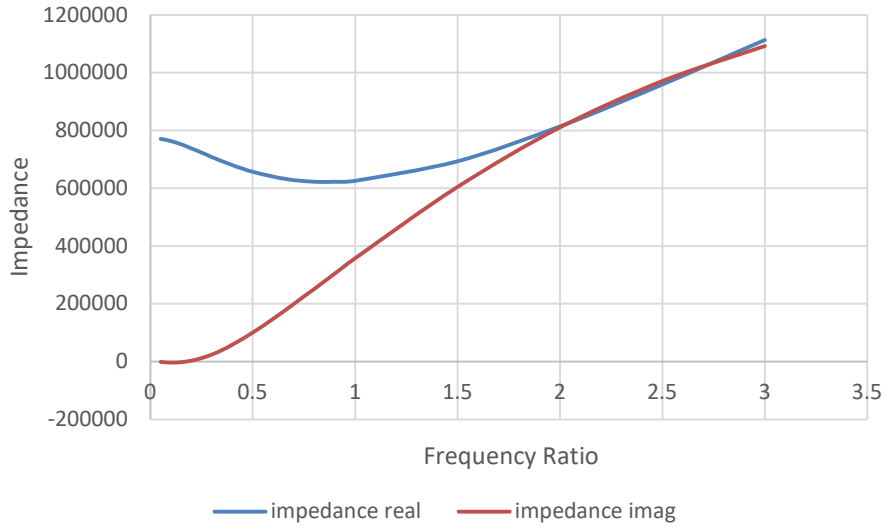

Figure 31 Impedance Curves of single pad bearing

Damped Natural Frequency Analysis

To determine the performance of the rotor bearing system from the stiffness and damping characteristics, damped natural frequencies and damping ratios are analysed. The details of the natural frequency analysis is explained in [9], and basic

principle is briefly explained. From Eq. (16), the real and imaginary parts of modal impedance are the modal stiffness and modal damping respectively.

In order to find the damped natural frequency, ω_d , the modal stiffness and $m\omega_s^2$ are plotted against the wide range of frequency ratios. The crossing point between the two curves is defined as ω_d , As shown in Figure 32, the crossing point defines the frequency ratio υ_n, K_{eq}, and damped natural frequency ω_n through Eq. (17).

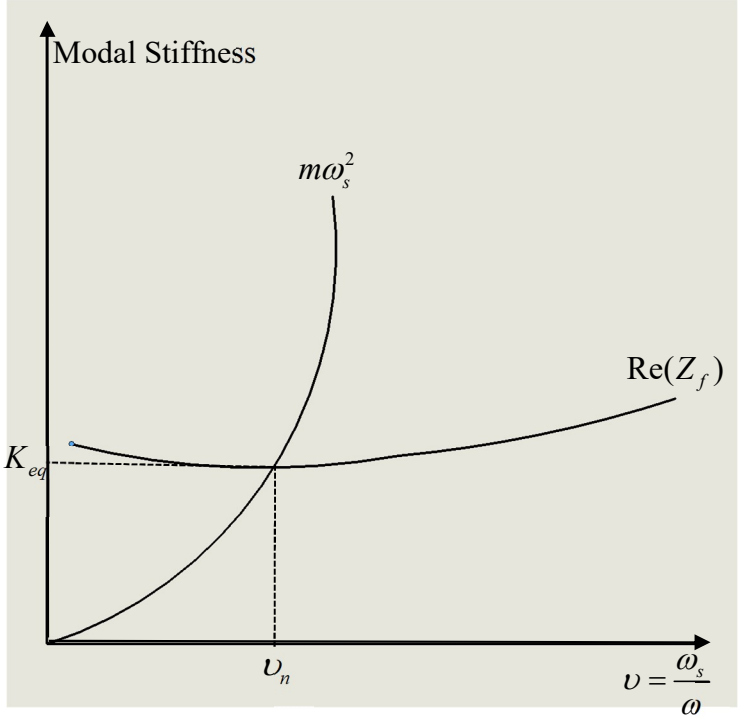

Figure 32 Definition of damped natural frequency and equivalent stiffness, Keq

$$\omega_n = \sqrt{\frac{K_{eq}}{m}} \tag{17}$$

The damping ratio can be determined by

$$\zeta = \frac{C_{eq}}{C_c} = \frac{C_{eq}}{2\sqrt{K_{eq} m}} \tag{18}$$

where,

$$C_c = 2\sqrt{K_{eq} m} = 2m\sqrt{\frac{K_{eq}}{m}} = 2m\omega_n \tag{19}$$

Figure 33 and Figure 34 present damped natural frequencies of a regular single pad bearing without shim and Case 1

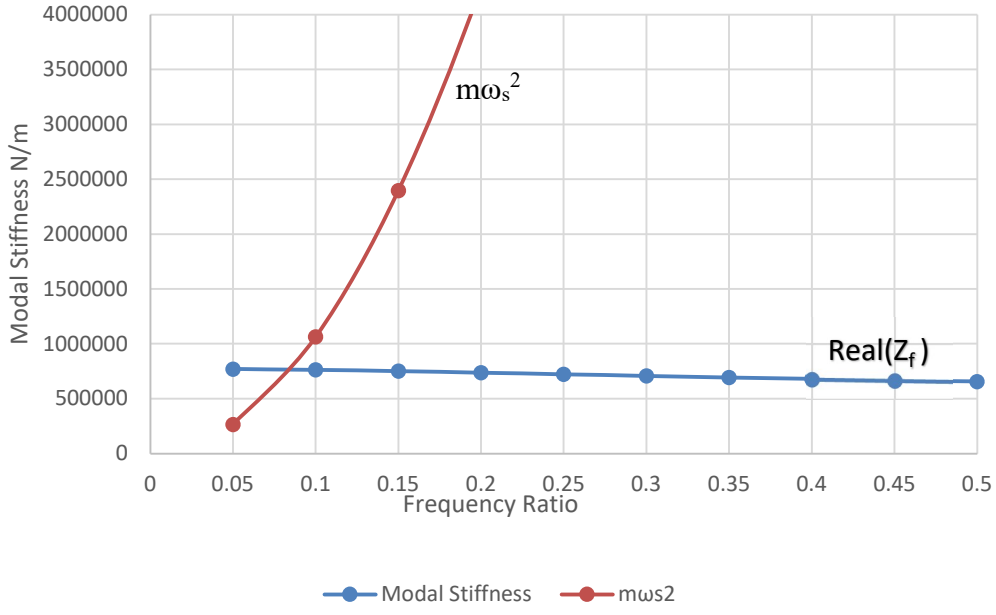

Figure 33 Modal stiffness and $m\omega_s^2$ vs frequency ratio at 36krpm for single pad bearing without shim

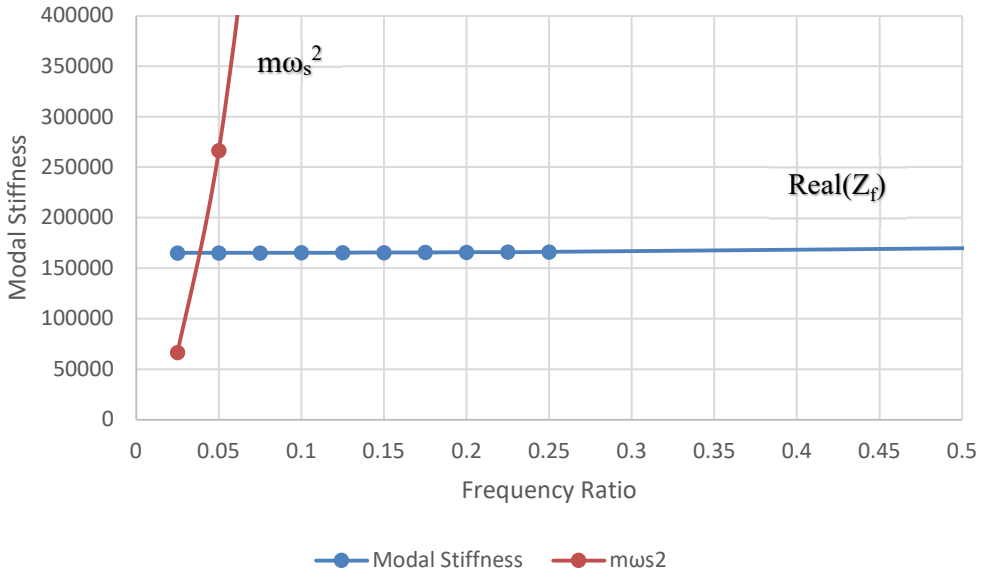

Figure 34 Modal stiffness and $m\omega_s^2$ vs frequency ratio at 36krpm for Case 3 bearing

Keq are about 1.2MN/m and 0.55MN/m for regular single pad bearing and shimmed bearing (Case 1), respectively. With the decrease in Keq, the damping

ratio increases and eventually the peak of the vibration decreases when the rotor is excited at the natural frequency.

Table 5 Summarizing the damped natural frequency and Keq from Case 1 to Case 4

Case Number	Natural Damped Frequency	Keq (N/m)	Damping Ratio	Modal Damping (Ceq)
1	185.923	261024.154	4.24	11868
2	158.267	202378.302	3.30	8124.3
3	140.770	165274.366	2.28	5086
4	192.246	279736.154	4.39	12731

From above Table 5, Case 3 has least Keq, damping ratio and natural damped frequency and modal damping showing not much difference with other cases. Therefore, Case 3 was chosen for further optimization of angular span of shims.

Effect of Shim Angular Span

The simulations were performed with varying shim angular span of each shim for all the shim locations cases. From the prelimanary simulations all the cases of location of the shims show similar pattern in the stiffness, damping and impednace

curves when the angular span is varied with each case. For every angular span case 3 is the best scenario for angular locations of the shims.

Modal damping tends to be low (sometimes negative if bearing is not designed properly) at low excitation frequencies. In addition, as can be seen in Figure 33 and Figure 34, typical range of ν_n is less than 0.1. Therefore, the modal stiffness and damping were evaluated at whirl frequency ratio of 0.05

The angular span is varied between 25° and 45°. From preliminary simulations, the minimum angular span was set to 25° because the cases with less than 25° does not result in any difference in the bearing characteristics. The maximum is taken as 45° because the shims start to overlap onto each other if the span is higher than 45°.

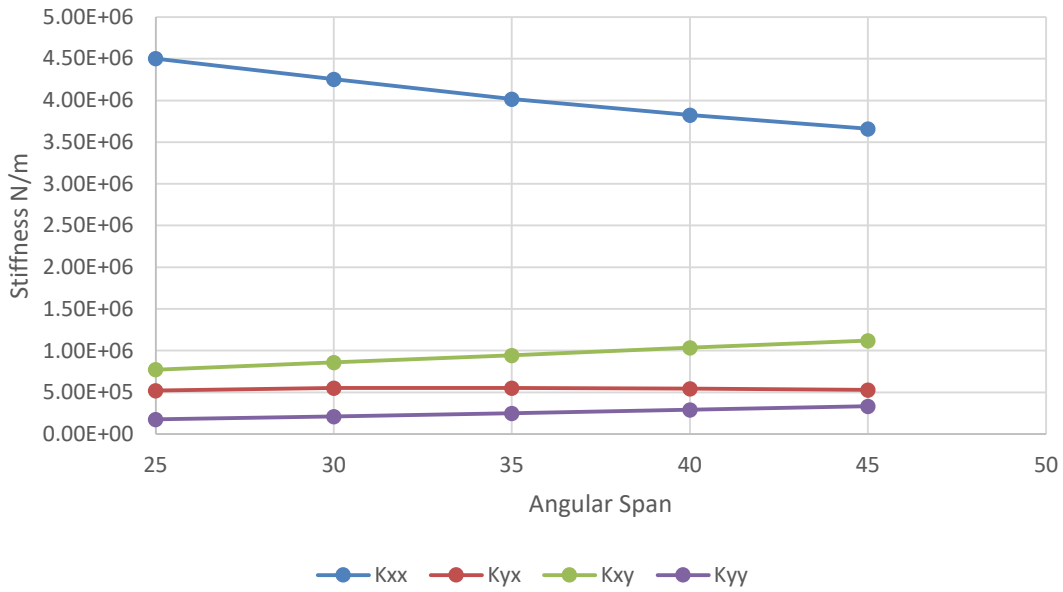

Figure 35 Stiffness coefficients with respect to angular span at $\nu = 0.05$.

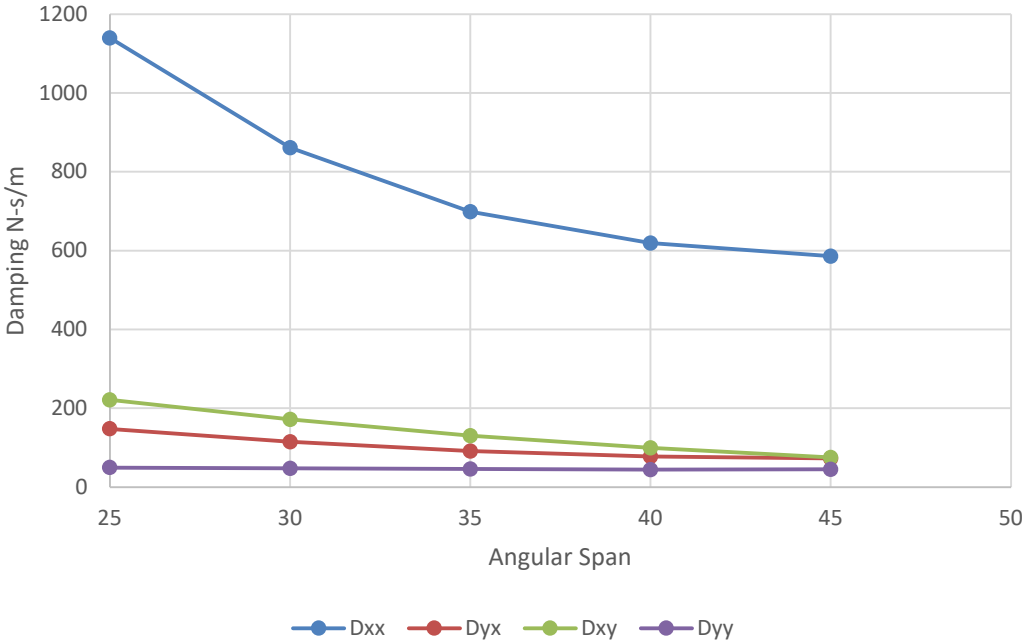

Figure 36 Damping coefficients vs Angular span graph at $\nu = 0.05$

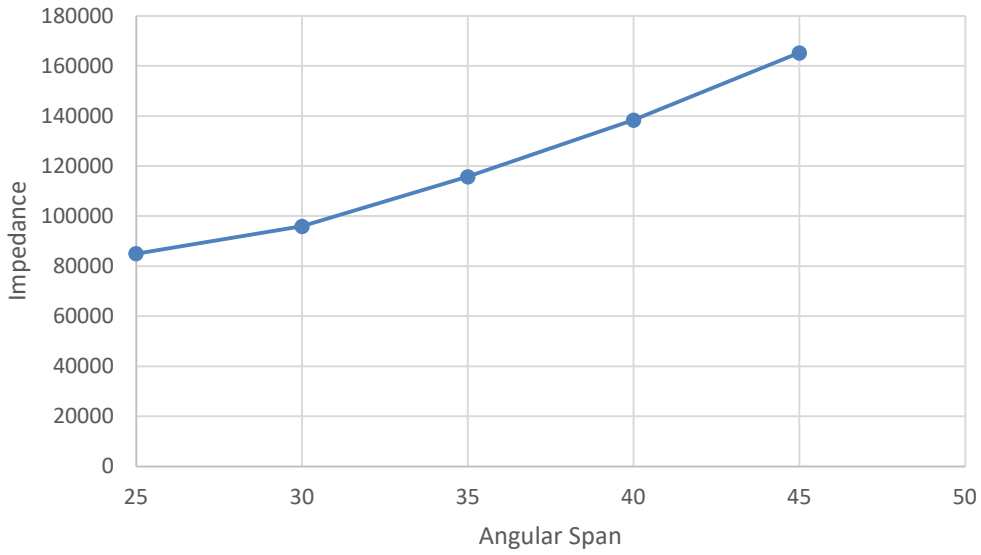

Figure 37 Modal Stiffness vs Angular span graph at $\nu = 0.05$

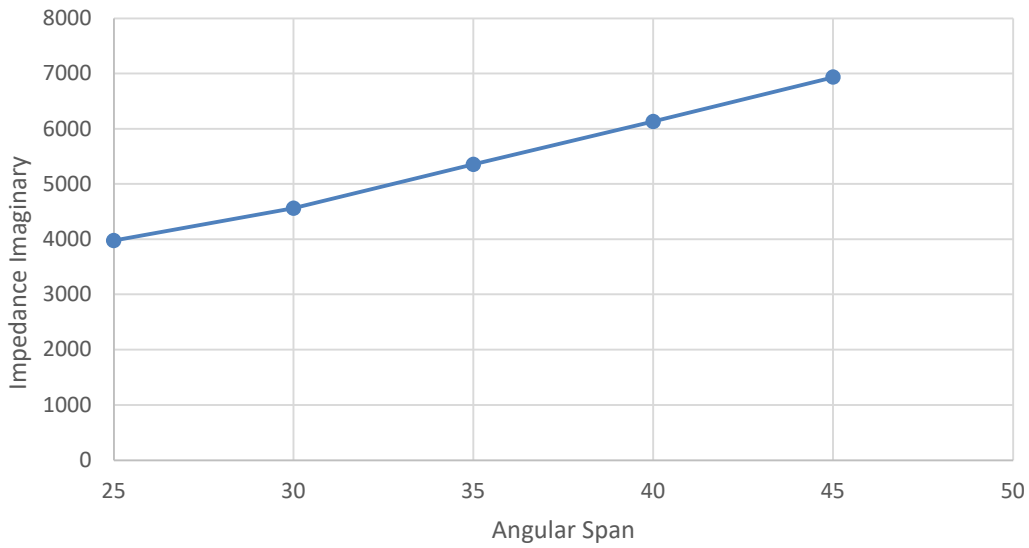

Figure 38 Modal Damping vs Angular span graph at $\nu = 0.05$

The modal stiffness and modal damping of the bearing increases with angular span as seen in Figure 37. The bearing with 45 degree angular span shows better modal damping when compared to all the other cases. To further improve the stability

charecteristics of the bearings, varying angular span of a shim in a bearing was simulated. The various cases that are simulated are given in Table 6.

Table 6 Shim angular spans with their locations following Case 3

Case No	Shim 1	shim 2	shim3
1	single pad bearing case		
2	25	25	25
3	30	30	30
4	35	35	35
5	40	40	40
6	45	45	45
7	30	45	30
8	30	50	30
9	45	30	45
10	50	30	50
11	50	45	50
12	60	30	60
13	60	45	60
14	3 pad bearing case		

Similar to the angular span variation, the frequency ratio of 0.05 was used to check the stability of each case. The variation of the stiffness, damping and impedance value with respect to each case is plotted in Figure 39~Figure 42.

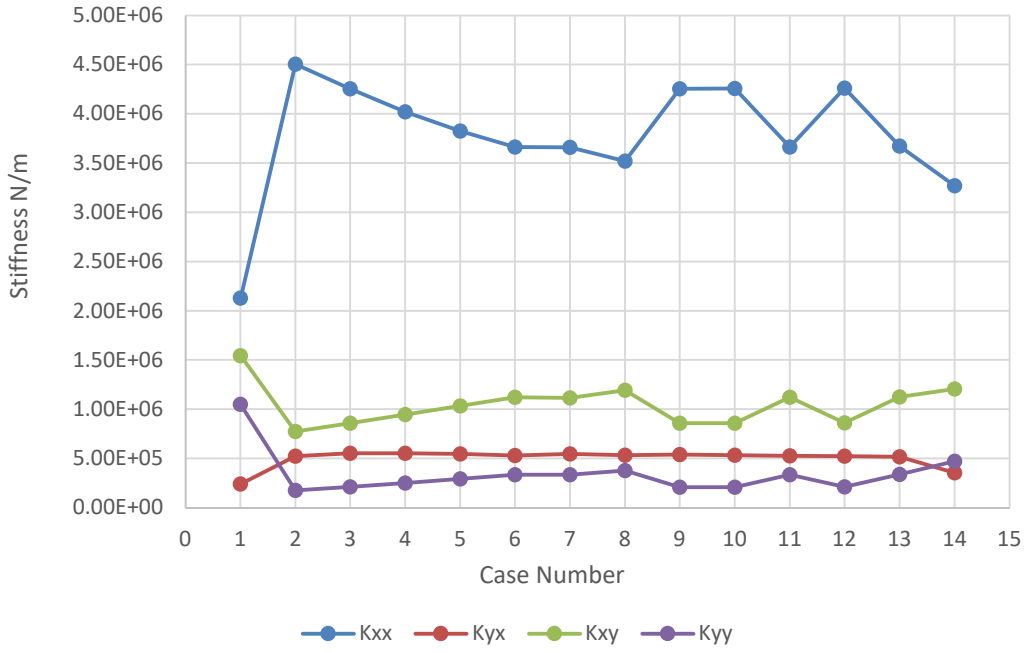

Figure 39 Stiffness coefficients of each case at ν=0.05

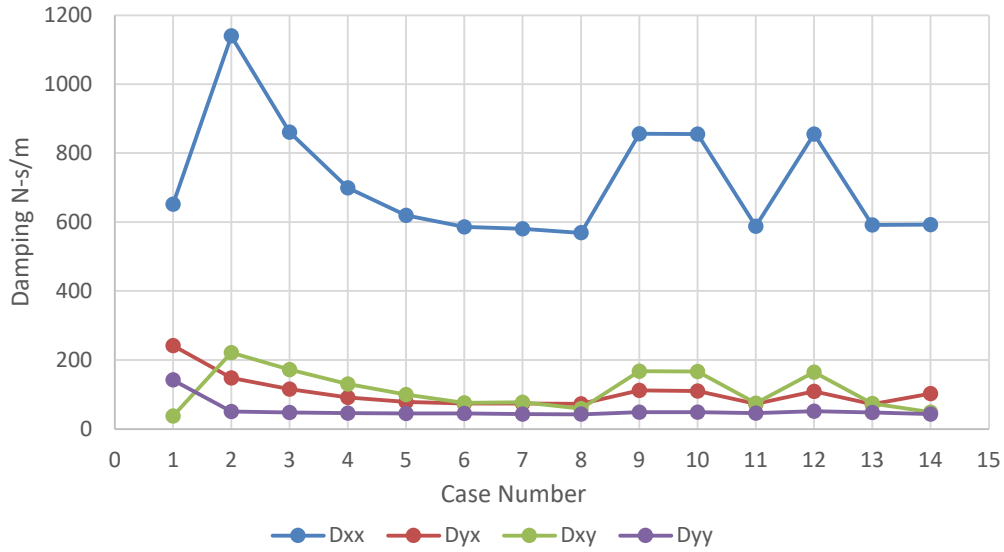

Figure 40 Damping coefficients of each case at ν=0.05

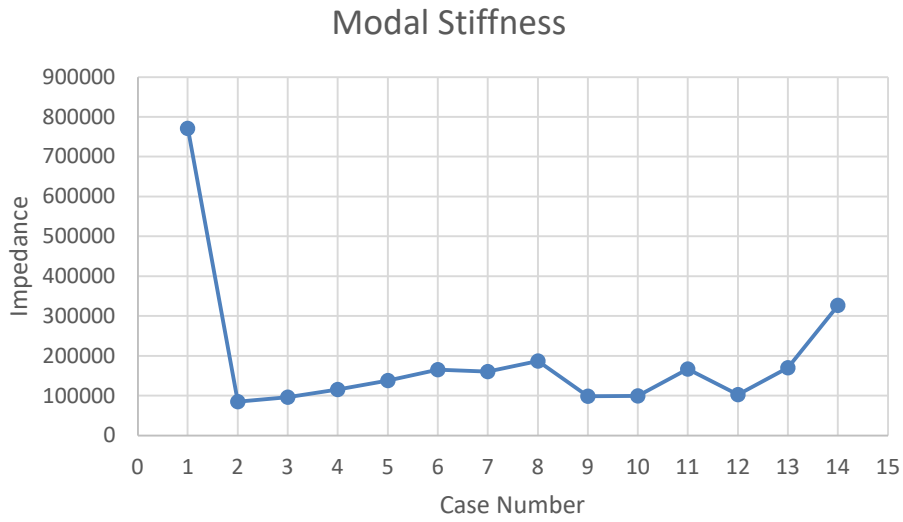

Figure 41 Modal Stiffness of each case at ν=0.05

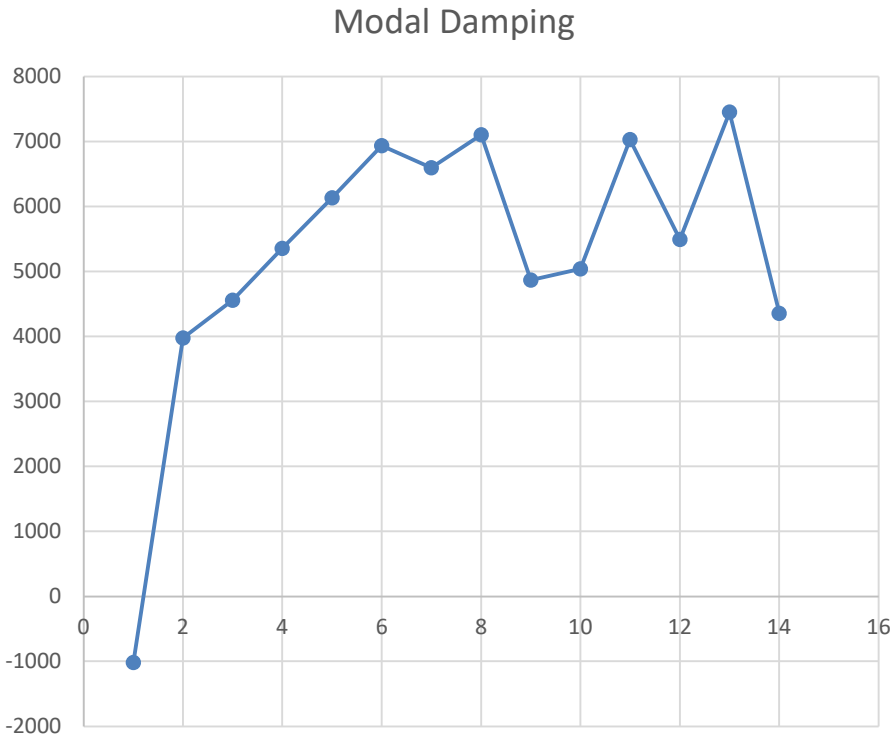

Figure 42 Modal Damping of each case at ν=0.05

Table 7 Keq, Ceq, Damping Ratio and Damped Natural Frequencies of 14 cases

Case Number	Keq	Ceq	Damping Ratio	ωs
1	766483.80	63877.00	1.33	306.39
2	85066.31	2256.10	1.41	102.95
3	95959.68	2708.80	1.60	108.08
4	115837.36	3299.50	1.77	117.46
5	138483.42	4089.20	2.01	128.14
6	165296.59	5086.00	2.28	140.78
7	160260.33	4804.40	2.19	138.41
8	187045.19	5631.30	2.38	151.04
9	98342.80	2888.60	1.68	109.21
10	99298.64	3006.10	1.74	109.66
11	166835.09	5294.40	2.37	141.51
12	102847.08	3369.40	1.92	111.33
13	170305.32	5645.20	2.50	143.14
14	327229.11	4691.90	1.50	202.82

Case 12 is selected as the best case because it has the less damped natural frequency, high damping ratio and high direct damping than most cases., From all the 14 configurations of the bearings which include three-pad and single pad bearing, Case 12 has overall better stability charecteristics.

Chapter 6 : CONCLUSION AND FUTURE WORK

Conclusion:

This paper investigates the effect of shims on the stiffness and damping coefficients of the bearing which inturn effect the stability charecterisstics of the bearing. Comparision of the three-pad and single pad bearings with various configurations of shimmed bearings is conducted through simulation. The shimmed bearings have better stability charecteristics than the single pad and three pad bearings. The single pad bearing has negative modal damping at $\nu = 0.05$. When shims are added, the modal damping is improved as it can be seen Figure 42. To further optimise the stability charecteristics and find the ideal design paramters of shims, the following steps are suggested,

1. Initially to determine the optimum paramters of the shims, the location of the shims which improve the stability charecteristics are found by simulating the bearing with various shims locations from Table 4.
2. The angular span of the shim which can improve the stability charecteristics of the bearing is found out by varying the angular span from 25^0 to 45^0.
3. To further improve the stability, bearing configurations variable angular spans are considered.

After the simulation are performed, case 12 was selected as the ideal case because of its least Keq value and the adequate modal damping when compared to other

configurations. The bearing used in the simulation is used in a 150kW turbo blower with a rotor mass of 7.5kg.

Future work:

The thesis presents the simulated results of stiffness and damping coefficients of the rotor-bearing system. To further get a clear idea of the stability of the bearing time orbit simulations can be perfornmed by solving the journal motions, bump deflections and unsteady Reynolds equation simultaneously. Rotordynamic analysis and imbalance response of the rotor can be included in the future work.

Chapter 7 : References

[1] Agrawal, Giri. (1997). Foil Air/Gas Bearing Technology — An Overview. 10.1115/97-GT-347.

[2] Ku, C. R., and Heshmat, H., 1992, "Compliant Foil Bearing Structural Stiffness Analysis: Part I---Theoretical Model Including Strip and Variable Bump Foil Geometry," J. Tribol., **114**, p. 2.

[3] Yazdi, B. Z., and Kim, D., 2018, "Rotordynamic Performance of Hybrid Air Foil Bearings With Regulated Hydrostatic Injection," J. Eng. Gas Turbines Power, **140**, p. 1.

[4] Yazdi, B. Z., and Kim, D., 2018, "Effect of Circumferential Location of Radial Injection on Rotordynamic Performance of Hybrid Air Foil Bearings," J. Eng. Gas Turbines Power, **140**(12), pp. 1–10.

[5] Radil, K., Howard, S., and Dykas, B., 2002, "The Role of Radial Clearance on the Performance of Foil Air Bearings," Tribol. Trans., **45**(4), pp. 485–490.

[6] Brasz, Joost J. "Investigation Into the Effect of Tip Clearance on Centrifugal Compressor Performance." Proceedings of the ASME 1988 International *Gas* Turbine and Aeroengine Congress and Exposition. Volume *1: Turbomachinery*. Amsterdam, The Netherlands. June 6–9, 1988. V001T01A066. ASME. https://doi.org/10.1115/88-GT-190

[7] Leader, M. E., Flack, R. D., and Allaire, P. E., 1979, “Experimental Study of Three Journal Bearings with a Flexible a Rotor,” ASLE Trans., **23**(4), pp. 363–369.

[8] Subbiah, R., and Littleton, J. E., 2018, *Rotor and Structural Dynamics of Turbomachinery*.

[9] Kim, D. (November 15, 2006). "Parametric Studies on Static and Dynamic Performance of Air Foil Bearings with Different Top Foil Geometries and Bump Stiffness Distributions." ASME. *J. Tribol*. April 2007; 129(2): 354–364. https://doi.org/10.1115/1.2540065

[10] Kim, D., 2018, “United States Patent,” United States Pat. US, **2**, p. 25.

[11] Schiffmann, J., and Spakovszky, Z. S., 2013, “Foil Bearing Design Guidelines for Improved Stability,” J. Tribol., **135**(1), pp. 1–11.

[12] Hoffmann, R., and Liebich, R., 2017, “Experimental and Numerical Analysis of the Dynamic Behaviour of a Foil Bearing Structure Affected by Metal Shims,” Tribol. Int., **115**(April), pp. 378–388.